

Article

Application of Intercriteria and Regression Analyses and Artificial Neural Network to Investigate the Relation of Crude Oil Assay Data to Oil Compatibility

Ivelina Shiskova ¹, Dicho Stratiev ^{1,2,*}, Mariana Tavlieva ¹, Angel Nedelchev ¹, Rosen Dinkov ¹, Iliyan Kolev ¹, Frans van den Berg ³, Simeon Ribagin ^{2,4}, Sotir Sotirov ⁵, Radoslava Nikolova ⁶, Anife Veli ⁶, Georgi Georgiev ¹ and Krassimir Atanassov ²

- ¹ LUKOIL Neftohim Burgas, 8104 Burgas, Bulgaria; shiskova.ivelina.k@neftochim.bg (I.S.); tavlieva.mariana.p@neftochim.bg (M.T.); kolev.iliyan.v@neftochim.bg (I.K.)
 - ² Institute of Biophysics and Biomedical Engineering, Bulgarian Academy of Sciences, Georgi Bonchev 105, 1113 Sofia, Bulgaria
 - ³ Black Oil Solutions, 2401 Alphen aan den Rijn, The Netherlands; bergberg134@gmail.com
 - ⁴ Department of Health and Pharmaceutical Care, University Prof. Dr. Assen Zlatarov, Professor Yakimov 1, 8010 Burgas, Bulgaria
 - ⁵ Laboratory of Intelligent Systems, University Prof. Dr. Assen Zlatarov, Professor Yakimov 1, 8010 Burgas, Bulgaria; ssotirov@btu.bg
 - ⁶ Central Research Laboratory, University Prof. Dr. Assen Zlatarov, Professor Yakimov 1, 8010 Burgas, Bulgaria
- * Correspondence: stratiev.dicho@neftochim.bg

Abstract: The compatibility of constituents making up a petroleum fluid has been recognized as an important factor for trouble-free operations in the petroleum industry. The fouling of equipment and desalting efficiency deteriorations are the results of dealing with incompatible oils. A great number of studies dedicated to oil compatibility have appeared over the years to address this important issue. The full analysis of examined petroleum fluids has not been juxtaposed yet with the compatibility characteristics in published research that could provide an insight into the reasons for the different values of colloidal stability indices. That was the reason for us investigating 48 crude oil samples pertaining to extra light, light, medium, heavy, and extra heavy petroleum crudes, which were examined for their colloidal stability by measuring solvent power and critical solvent power utilizing the n-heptane dilution test performed by using centrifuge. The solubility power of the investigated crude oils varied between 12.5 and 74.7, while the critical solubility power fluctuated between 3.3 and 37.3. True boiling point (TBP) analysis, high-temperature simulation distillation, SARA analysis, viscosity, density and sulfur distribution of narrow petroleum fractions, and vacuum residue characterization (SARA, density, Conradson carbon, asphaltene density) of the investigated oils were performed. All the experimentally determined data in this research were evaluated by intercriteria and regression analyses. Regression and artificial neural network models were developed predicting the critical solubility power with correlation coefficients R of 0.80 and 0.799, respectively.

Keywords: oil colloidal stability; petroleum; asphaltenes; SARA; intercriteria analysis; regression; ANN



Citation: Shiskova, I.; Stratiev, D.; Tavlieva, M.; Nedelchev, A.; Dinkov, R.; Kolev, I.; van den Berg, F.; Ribagin, S.; Sotirov, S.; Nikolova, R.; et al. Application of Intercriteria and Regression Analyses and Artificial Neural Network to Investigate the Relation of Crude Oil Assay Data to Oil Compatibility. *Processes* **2024**, *12*, 780. <https://doi.org/10.3390/pr12040780>

Academic Editor: Liang Zhang

Received: 21 March 2024

Revised: 8 April 2024

Accepted: 11 April 2024

Published: 12 April 2024



Copyright: © 2024 by the authors. Licensee MDPI, Basel, Switzerland. This article is an open access article distributed under the terms and conditions of the Creative Commons Attribution (CC BY) license (<https://creativecommons.org/licenses/by/4.0/>).

1. Introduction

Twenty-four years ago, Wiehe and Kennedy postulated the oil compatibility model [1,2]. It was derived on the basis of two hypotheses: (1) the polynuclear condensed aromatic and naphthenic ring structures with attached alkyl groups and heteroatoms (sulfur, oxygen, nitrogen, metals), frequently defined as solubility class asphaltenes, precipitate at the same blend solubility parameter regardless of whether the oil is commingled with another oil or a hydrocarbon liquid; (2) the blending solubility parameter is calculated following the lineal mixing volume rule [1]. By employing the solvent–anti-solvent pair (toluene/n-heptane) and performing toluene equivalent and heptane dilution tests, the solubility and insolubility

numbers have been determined [3]. Wiehe has applied the oil compatibility model in several studies, proving its viability [4–6]. The same principle of using the solvent–anti-solvent pair was set in the standards of ASTM D 7112 (p -value) [7], ASTM D 7157 (S-value) [8], and ASTM D 7061 (separability number) [9]. Wiehe [3] applied a manual procedure (microscope) to define the flocculation point during the titration of oil/toluene blends with heptane, while the standardized methods mentioned above use an optical device to determine it [7–9]. Frans van den Berg reviewed the historical development of dual-solvent titration methods over the years with some specific applications of these methods [10]. The standardized methods ASTM D 7112 [7], ASTM D 7157 [8], and ASTM D 7061 have been applied in oil refining to monitor the performance of vacuum residue conversion processes [11]. While in high-conversion vacuum residue processes like ebullated bed hydrocracking the insolubility number expressed by $1-S_a$ (S_a = asphaltene solubility determined by the ASTM D 7157 standard) can be very high = 0.70, in visbroken residues, it can be about 0.50, and in crude oils, it can oscillate between 0.16 and 0.42 [11,12]. These data suggest that the incompatibility of crude oils can be mainly because of the low oil solubility power instead of the high insolubility number of asphaltenes. This deduction is supported by the results reported by Rogel et al. [13] showing a crude oil with a very high fouling propensity, whose very low p -value = 0.98 is due to the very low oil solubility power ($P_o = 0.25$) regardless of the relatively low insolubility number ($1 - P_a = 0.265$). This can explain why light crude oils are reported by some authors to be more prone to cause asphaltene precipitations than heavy oils [14–17]. Apart from the abovementioned methods, various predictive models and experimental techniques have been implemented to estimate oil stability throughout the years, such as the colloidal instability index (CII) [18–21], colloidal stability index (CSI) [19,21,22], stability index (SI) [19,22,23], Stankiewicz plot (SP) [19,21,24], qualitative–quantitative analysis (QQA) [21], stability cross plot (SCP) [21,25], Heithaus parameter (or parameter P) [26], heptane dilution (HD) [27,28], toluene equivalence (TE) [3,29,30], spot test [26,31–35] and separability number (SN) [26,36,37], Jamaluddin method (JM) [38–40], modified Jamaluddin method (MJM) [41], density-based asphaltene stability envelope (DBASE) [19], in-line filtration method [42], 1D low-field nuclear magnetic resonance relaxometry and chemometric methods [43,44], and the viscometric determination of the onset of asphaltene flocculation [45–48]. The advantage of using these predictive models is that they are simple, need a very small amount of input data, and do not have computational complexities. Nevertheless, the results obtained by these methods may vary a lot depending on the test method used and do not coincide with each other [21,23,26,42]. Ali et al. [49] demonstrated that the methods based on SARA analysis (SI, JM, MJM, CSI, SP) could show a poor performance in predicting stable and unstable samples, while the results obtained from the experimental methods are affected by the type of procedure, stability judgement criteria, and human error. Likewise, Guzmán et al. [26] point out that the correlations reported in the literature are not adequate when they are used individually to establish limits on asphaltene stability in crude oils and that they have low effectiveness for stability prediction. Therefore, researchers continue their search in an attempt to find a suitable approach for predicting crude oil stability [50–67]. The viscosity of crude oil to be examined by the oil compatibility tests also needs to be taken into account [10,68–70]. However, the full analysis of the examined petroleum fluids has not been juxtaposed with the compatibility characteristics in these research articles that could provide an explanation for the different values of colloidal stability indices. That was the reason for us choosing to investigate 48 crude oil samples pertaining to extra light ($SG < 0.8017$), light ($0.8017 < SG < 0.855$), medium ($0.855 < SG < 0.922$), heavy ($0.922 < SG < 1.00$), and extra heavy petroleum crudes ($SG > 1.00$), which were examined for their colloidal stability by the procedure described in [65,66]. In this procedure, the solvent power and critical solvent power [34] of the studied petroleum fluids are determined. True boiling point (TBP) analysis, high-temperature simulation distillation, SARA analysis, the density and sulfur distribution of narrow petroleum fractions, and vacuum residue characterization (SARA, density, Conradson carbon, asphaltene density) were performed

of the investigated oils. All experimentally determined data in this research were evaluated by intercriteria, regression analyses, and an artificial neural network to seek statistically meaningful relations between petroleum properties and compatibility characteristics, and to develop regression and ANN models to predict oil compatibility. The aim of this paper is to discuss the obtained results.

2. Materials and Methods

Samples of forty-seven crude oils, and an atmospheric residue, derived from forty-two crude oils were investigated in this research. The bulk properties of the studied petroleum crudes are presented in Table 1.

Table 1. Density, sulfur, viscosity, and SARA composition of investigated crude oils.

No	Crude Oil Sample Name	D ₁₅ , g/cm ³	Kin. Viscosity at 40 °C, mm ² /s	Sulphur, wt.%	T50% (TBP), °C	Saturates, wt.%	Aromatics, wt.%	Resins, wt.%	C ₇ -asp., wt.%	C ₅ -asp., wt.%
1	Albanian	1.0014	2090	5.64	442	24.5	56.3	6.6	12.6	19.2
2	Arabian Light	0.8581	6.3	1.89	353	61.5	35.1	2	1.4	3.4
3	Arab. Med.–1	0.868	9.8	2.4	366	57.1	39.5	2.1	1.3	3.4
4	Arab. Med.–2	0.8703		2.45	372					
5	Arab Heavy	0.8916	17.3	2.967	408	52.1	40.7	2.8	4.4	7.3
6	Aseng	0.8741	8.6	0.258	358	56.5	41.6	1.8	0.1	1.9
7	Azery Light	0.8483	4.5	0.2	323	64.6	34.7	0.66	0.04	0.13
8	Basrah Light–1	0.884	10.9	3.31	390	55.3	39.5	2.5	2.7	5.1
9	Basrah Light–2	0.8772		2.94	385					
10	Basrah Med.–1	0.8876	12.5	3.36	400	52.5	38.9	6	2.6	3.4
11	Basrah Med.–2	0.8836		3.1	389					
12	Basrah Heavy	0.9133	24.6	4.08	433	47.5	43.7	3.2	5.6	8.8
13	Boscan	0.9953	14953	4.77	558	24.3	59.6	4.6	11.5	16.1
14	Buzachi	0.9065	84.2	1.571	450	47	50.2	1.9	0.9	2.9
15	Cheleken	0.8469	12.1	0.4	345	65	32.8	1.8	0.4	2.2
16	CPC–1	0.7954	1.8	0.55	237	82.7	15.3	1.96	0.04	0.14
17	CPC–2	0.7993		0.53	238					
18	CPC–3	0.801		0.56	238					
19	El Bouri	0.8913	20.9	1.72	403	51.5	43	2.5	3	5.5
20	El Sharara	0.814	2.7	0.08	253	76.1	22	1.8	0.11	0.5
21	Forties	0.817	4.4	0.679	264	75.1	23	1.7	0.2	0.5
22	Helm_1.2022	0.935	92.4	1.71	448	39.6	54.1	2.6	3.7	6.3
23	Helm_1.2024	0.9348		1.63	455	39.6	53.2	2.9	4.3	7.1
24	Johan Sverdrup	0.8867	12.2	0.82	390	52.7	43	2.3	2	4.2
25	Kazakh	0.8777	6.5	0.4	426	61.5	36.2	1.8	0.5	2.3
26	Kirkuk	0.8538	6.4	2.26	332	56.8	38.7	2.3	2.2	4.5
27	Kirkuk AR	0.9586	316	2.98	531	33.8	54.6	4.7	6.9	11.6
28	Kumkol	0.8209	4.3	0.22	324					
29	Kuwait Export	0.8729	12.2	2.69	390	55.9	39	2.4	2.7	5.1
30	Kuwait Light	0.8313	2.4	1.049	289	70.2	27.2	1.6	1	1.6
31	Okwuibome	0.8676	7.2	0.202	309	58.5	39.6	1.85	0.05	0.15
32	Oryx	0.9156	123.2	4.209	448	44.6	42.9	3.9	8.6	12.5
33	Prinos	0.875	5.5	3.71	345	56.2	37.5	2.7	3.6	6.3
34	Ras Gharib	0.9256	95	3.44	486	41.9	48.6	3.3	6.2	9.5
35	REBCO–1	0.874	12.6	1.44	386	55.6	40.5	2.2	1.7	3.8
36	REBCO–2	0.8755		1.49	390					
37	Rhemoura	0.8648	7.5	0.75	342	59.3	35.8	2.3	2.6	4.9
38	Sepia	0.8883	25.9	0.41	430	52.3	44.6	2	1.1	3.1
39	Sib. Light	0.8538	6.2	0.57	348	62.7	34.4	2	0.9	2.9
40	SGC	0.8827	27.6	2.26	406	53.8	40.6	2.5	3.1	5.6
41	Tartaruga	0.893	17.1	0.73	415	50.4	45.9	2.1	1.6	3.7
42	Tempa Rossa	0.9401	62	5.35	455	38.3	49.1	3.9	8.7	12.6
43	Vald’Agri	0.8323	3.2	1.96	280	69.8	26.6	2.8	0.8	3.6
44	Varandey	0.8503	6.1	0.625	336	64	32.8	2	1.2	3.2
45	Western Desert	0.8208	2.16	0.26	266	73.7	22.5	3.1	0.7	1.3
46	Es Sider	0.8382	4.85	0.415	321	67.9	28.5	3.1	0.5	3.6
47	Payra Gold	0.8849	14	0.685	380	53.3	41.9	4.6	0.2	1.8
48	KEBCO	0.8741	10.8	1.7	373	56.5	39	1.7	2.8	4.5
	Min	0.7954	1.8	0.08	237	24.3	15.3	0.66	0.04	0.13
	Max	1.0014	14,953	5.64	558	82.7	59.6	6.6	12.6	19.2

2.1. Analytical Procedures for Crude Oil Assay

The density of the studied crude oils and their fractions were measured by the use of the digital analyzer Anton Paar equipped with a U-shaped oscillating tube, electronic excitation system, and temperature control system according to the requirements of the standard method ASTM D4052 [71]. An energy dispersive X-ray fluorescence analyzer, manufactured by Tanaka Scientific, was used to determine the sulfur content of the studied

petroleum oils and their distillate cuts by applying method ASTM D 4294 [72]. An in-house analytical procedure [11] based on the solubility of the petroleum fractions in different organic solvents was used to assign SARA analysis of vacuum residues. The asphaltene density was assessed by a dilution procedure, with toluene described in detail in [73]. The standard method IP-501/05 based on inductively coupled plasma emission spectrometry was applied to measure the metal contents (Ni, V, Na, etc.) of the crude oils [74].

Crude oil fractions and TBP distillation characteristics were obtained by the standard procedures described in ASTM D2892 [75] and ASTM D5236 [76] in ROFA automatic crude oil distillation systems (15-theoretical plate column and vacuum pot still system). Also, high-temperature gas chromatography was applied to determine the boiling point distribution of the studied oil samples according to ASTM D7169 [77].

2.2. Compatibility Indexes and Models for Crude Oil Colloidal Stability Prediction

2.2.1. Compatibility Model of Nemana et al.

The predictive crude oil compatibility model of Nemana et al. [65] was used to assess the colloidal stability of the investigated 48 petroleum samples. Nemana et al.'s predictive model comprises the assignment of solvent power (Sp) and critical solvent power (Sp critical). The analytical procedure includes the determination of heptane insolubles by centrifugation, boiling point, and density assays. The crude oil Sp was estimated as described in [65], and it is shown in Equation (1).

$$Sp = \frac{K_{CO} - K_H}{K_T - K_H} \times 100 \quad (1)$$

where

K_{CO} —characterization factor of crude oil;

K_H —characterization factor of n-heptane = 12.72 [66];

K_T —characterization factor of toluene = 10.15 [66].

Boiling point distribution according to the high-temperature simulation distillation (ASTM D 7169) and density (D15) of each crude oil was used to calculate the Watson characterization factor (K_w) (Equation (2)).

$$K_W = \left(\frac{\sqrt[3]{Meabp}}{D15} \right) \quad (2)$$

where

$Meabp$ —mean average boiling point, °R.

The initial sediment precipitation point determined by the dilution test with n-heptane was used to estimate the critical solvent power of each studied crude oil. The Sp critical was calculated by Equation (3) using the K_w of the blend of petroleum/n-heptane at the sludge settling point.

$$Sp \text{ critical} = \frac{K_{ch} - K_H}{K_T - K_H} \times 100 \quad (3)$$

where

K_{ch} —characterization factor of the blend petroleum/n-heptane at the point of initial sludge settling.

The solvent power of the petroleum blends (SP blend) was estimated by the linear mixing rule using the weight part (x_i) and Sp of each crude oil in the mixture, as shown in Equation (4):

$$Sp \text{ blend} = \sum (x_i \times Sp_i) \quad (4)$$

The relative compatibility index (RCI) introduced by Ancheyta [34] was applied to evaluate the compatibility of the petroleum blends (Equation (5)). The petroleum blend is considered compatible when the $RCI > 1$.

$$RCI = \frac{Sp_{blend}}{Sp_{critical\ max}} > 1 \quad (5)$$

where

$Sp_{critical\ max}$ —maximum value of the critical solvent power of the petroleum blends that are part of the mixture.

2.2.2. Modified Compatibility Model of Nemana et al.

For the purpose of the current investigation, the Nemana et al. procedure was modified as follows:

- Characterization factor was estimated using the evaporation temperature of 50% of crude oil from TBP distillation— $T_{50\%}$;
- Characterization factor of the blend petroleum/n-heptane at the point of initial sludge settling was calculated using Equation (6) as described in [78–83].

$$K_{ch} = x_{co} \times K_{co} + x_H \times K_H \quad (6)$$

where

x_{co} —weight part of crude oil in the blend petroleum/n-heptane;

x_H —weight part of n-heptane in blend petroleum/n-heptane at the initial sediment precipitation point.

2.2.3. Colloidal Instability Index

The colloidal instability index (CII) is a widely used method for asphaltene colloidal stability evaluation [18–21]. The colloidal instability index was calculated by using Equation (7) and the data of the pseudocomponent saturates (Sat), aromatics (Aro), resins (Res), and asphaltene ($Asph$) consisted in the crude oil.

$$CII = \frac{Sat + Asph}{Aro + Res} \quad (7)$$

2.2.4. Oil Compatibility Model

Wiehe and Kennedy [1] introduced the oil compatibility model that includes two reduced-solubility parameters: solubility blending number (S_{BN}) and insolubility number (I_N). The S_{BN} of each crude oil was estimated using Equation (8) and the solubility parameter values of crude oil (δ_{CO}), toluene ($\delta T = 18.3 \text{ MPa}^{0.5}$), and n-heptane ($\delta H = 15.2 \text{ MPa}^{0.5}$) [65]. A correlation reported by Corraera et al. [84] (Equation (9)) and crude oil density at 20 °C (d) was applied to determine the crude oil solubility parameter.

$$S_{BN} = 100 \left[\frac{\delta_{CO} - \delta H}{\delta T - \delta H} \right] \quad (8)$$

$$\delta_{CO} = 24.042 * d^{0.5} - 4.5989 \quad (9)$$

The ratio $\frac{S_{BN}}{I_N}$ was directly determined by the dilution test with n-heptane and Equation (10). The point without precipitating asphaltene at a maximum volume of n-heptane (Vh , mL) at a certain volume of oil ($Voil$, mL) was used to compute the ratio $\frac{S_{BN}}{I_N}$.

$$\frac{S_{BN}}{I_N} = 1 + \frac{Vh}{Voil} \quad (10)$$

The solubility blending number of the crude oil blends (S_{BNmix}) was estimated by applying Equation (11) [65].

$$S_{BNmix} = \frac{\sum V_i * S_{NBi}}{\sum V_i} \quad (11)$$

where

V_i —volume of i crude oil in the blend, mL;

S_{NBi} —solubility number of i crude oil in the blend.

The crude oil mixture is considered to be compatible when the solubility parameter of the petroleum blend (S_{BNmix}) is higher than the flocculation solubility parameter of each oil component (I_{Nmax}), as shown in Equation (12):

$$S_{BNmix} > I_{Nmax} \quad (12)$$

2.3. Intercriteria Analysis

The intercriteria analysis (ICrA) theory well described in references [85–87] is based on intuitionistic fuzzy sets and index matrices. As incoming data, ICrA needs $m \times n$ table of observations or scores of m objects on n criteria. It recalls a $n \times n$ table of intuitionistic fuzzy pairs determining the grades of the relationship between each pair of criteria, hence the name “intercriteria”. In the interest of terminological precision, the ICrA avoids the term “correlation” between criteria and instead uses the terms “positive consonance”, “negative consonance”, and “dissonance”. In ICrA, a second function $\nu_A(x)$ is instilled in intuitionistic fuzzy sets to determine, respectively, the non-membership of the element x to the set A , which can co-exist with the membership function $\mu_A(x)$, both having values in the interval $[0; 1]$. For $\mu = 0.75 \div 1.00$ and $\nu = 0 \div 0.25$, a region of statistically meaningful positive consonance is obtained, whereas at $\mu = 0 \div 0.25$ and $\nu = 0.75 \div 1.00$, an area of statistically meaningful negative consonance is derived. All other cases are considered to be dissonance. A comprehensive description of ICrA application in oil refining is given in [88].

3. Results and Discussion

3.1. Heptane Dilution Test Results

Figure 1 shows a graphical presentation of n-heptane dilution tests performed with extra light, light, medium, and heavy crudes.

The data in Figure 1 show that the flocculation starts at a different content of n-heptane in the blend with diverse crude oils. As discussed in the work of Guzman et al. [26], crude oils with a low asphaltene content encounter difficulties in determining the onset of asphaltene precipitation. This is confirmed with the graphs in Figure 1a–c indicating no precipitation of asphaltenes during the n-heptane dilution test with the extra light and light crude oils.

Table 2 summarizes the obtained values of the RCI, modified RCI, solubility blending, and insolubility numbers, the content of n-heptane indicating the beginning of asphaltene precipitation, and the solubility parameter of the investigated petroleum oils. The range of the variation in all the oil parameters reported in Table 2 shows that it is wide enough to use these data for statistical analysis. To study the relations between the different n-heptane-based oil compatibility indices, ICrA evaluation was performed. Tables 3 and 4 present the μ -values and ν -values of the ICrA evaluation of the data in Table 2.

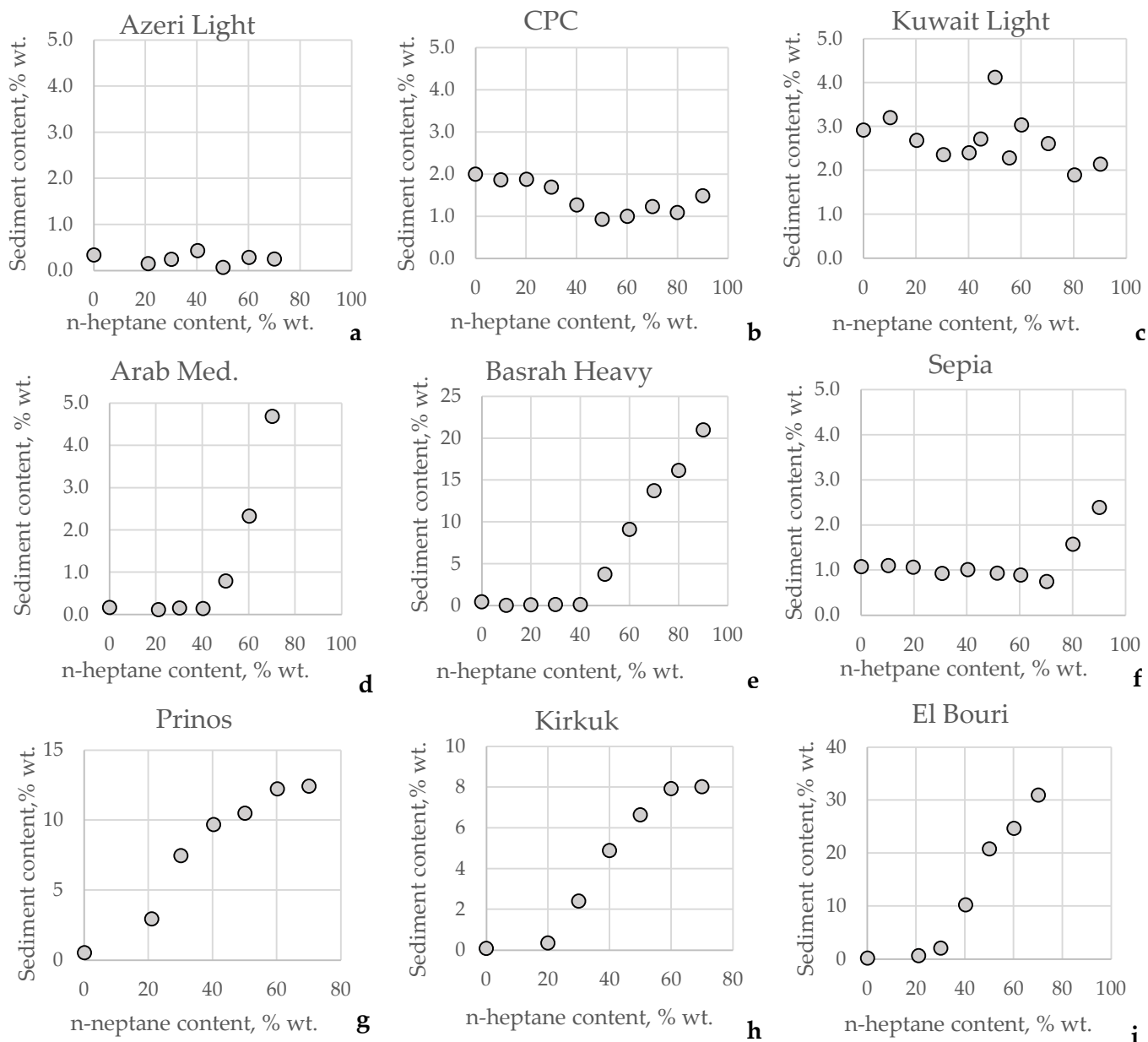


Figure 1. Crude oil sediment content relation to n-heptane content in the blend crude oil–n-heptane for the crude oils Azeri Light (a); CPC blend (b); Kuwait Light (c); Arab. Medium (d); Basrah Heavy (e); Sepia (f); Prinos (g); Kirkuk (h); El Bouri (i).

Table 2. Compatibility indices of studied crude oils.

No	Crude Oil Name	Sp	Sp cr.	RCI	Kw	Kw Blend	Sp (Mod.)	Sp cr. (Mod)	RCI (Modified)	n-Heptane Content in the Crude Oil, wt.% (at Onset of Asphaltene Precipitation)	SBN/IN	SBN	IN	δCO	CII(C7)	CII(C5)
1	Albanian	93.5	53	1.8	10.85	11.82	74.7	37.3	2	50	2	137	69	19.5	0.59	0.78
2	Arabian Light	35.6	27.2	1.3	12.11	12.38	26.1	15.6	1.7	40	1.6	80	51	17.7	1.70	1.85
3	Arab. Med-1	43.1	37.1	1.2	12.06	12.39	28.1	15.5	1.8	45	1.7	84	49	17.8	1.40	1.53
4	Arab. Med-2	49.6	35.1	1.4	12.07	12.47	27.8	12.5	2.2	55	2.1	85	41	17.8		
5	Arab Heavy	59.9	33.5	1.8	11.99	12.43	30.7	13.8	2.2	55	2.1	94	45	18.1	1.30	1.46
6	Aseng	43.3	26.8	1.6	11.93	12.31	33.3	18.3	1.8	45	1.7	86	50	17.9	1.30	1.40
7	Azery Light	43.3	1.2	12.06	12.35	28.3					1.6	76	48	17.5	1.83	1.84
8	Basrah Light-1	51.9	36.7	1.4	11.99	12.39	30.9	15.4	2	50	1.9	91	48	18	1.38	1.53
9	Basrah Light-2	50.8	42.7	1.2	12.05	12.42	28.6	14.3	2	50	1.9	88	47	17.9		
10	Basrah Med-1	37.2	29.7	1.3	12	12.36	30.4	16.7	1.8	45	1.7	92	53	18.1	1.23	1.27
11	Basrah Med-2	50.8	42	1.2	11.99	12.35	31	17.1	1.8	45	1.7	90	52	18		
12	Basrah Heavy	63.7	47.4	1.3	11.85	12.32	36.3	18.1	2	50	1.9	102	54	18.4	1.13	1.29
13	Boscan	69.5	47.9	1.5	11.48	12.4	50.5	15.1	3.3	70	3.3	135	41	19.4	0.56	0.68
14	Buzachi	45	35.8	1.3	12.04	12.45	29.1	13.1	2.2	55	2.1	100	47	18.3	0.92	1.00
15	Cheleken	36.8	22.8	1.6	12.22	12.56	21.8	21.8	2.5	60	2.3	75	33	17.5	1.89	2.05
16	CPC-1	22.1	1	12.21	12.33	22.3					1.2	53	44	16.8	4.79	4.83
17	CPC-2	35.6	1.2	12.16	12.36	24.4					1	55	55	16.9		
18	CPC-3	29.9	1	12.13	12.13	25.3					1	55	55	16.9		
19	El Bouri	42.8	39.5	1.1	11.97	12.21	31.7	22.2	1.4	30	1.4	94	68	18.1	1.20	1.33
20	El Sharara	28	13.9	2	12.05	12.58	28.5	8	3.6	72	3.1	61	20	17.1	3.20	3.27
21	Forties	37.8	18.7	2	12.09	12.45	27	13.2	2	51	1.9	62	34	17.1	3.05	3.10
22	Helm_1.2022	52.6	30.2	1.7	11.65	12.22	43.8	21.9	2	50	1.9	111	57	18.6	0.76	0.85
23	Helm_1.2024	59.5	43	1.4	11.7	12.3	42.2	19	2.2	55	2.1	111	52	18.6	0.78	0.88
24	Johan Sverdrup	45.8	34.3	1.3	11.95	12.46	32.3	12.6	2.6	61	2.4	92	38	18	1.21	1.32
25	Kazakh	29.5	16.2	1.8	12.29	12.49	19.3	11.6	1.7	40	1.6	88	55	17.9	1.63	1.76
26	Kirkuk	45	41.5	1.1	12.04	12.19	28.8	23	1.3	20	1.2	78	64	17.6	1.44	1.58
27	Kirkuk AR	55	34.1	1.6	11.79	12.29	38.5	19.3	2	50	2	121	62	18.9	0.69	0.83
28	Kumkol	38.1	37.4	1	12.47	12.5	12.5	11.2	1.1	10	1.1	64	59	17.2		
29	Kuwait Export	55.2	41.8	1.3	12.14	12.4	25.1	15.1	1.7	40	1.6	86	54	17.9	1.42	1.56
30	Kuwait Light	37.7	1	12.07	12.43	27.8					1.8	68	37	17.3	2.47	2.55
31	Okwuibome	48.4	28.1	1.7	11.7	12.24	42.1	21	2	50	1.8	84	45	17.8	1.41	1.42
32	Oryx	59.7	49.9	1.2	11.9	12.21	34.2	22.2	1.5	35	1.5	103	69	18.4	1.14	1.33
33	Prinos	60.2	38.2	1.6	11.83	11.98	36.9	31.3	1.2	15	1.2	87	75	17.9	1.49	1.67
34	Ras Gharib	47	21.5	2.2	11.98	12.3	31.2	18.7	1.7	40	1.6	107	66	18.5	0.93	1.06
35	REBCO-1	47.8	31.9	1.5	12.1	12.51	10.6	2.5	60	2.3	86	37	17.9	1.34	1.46	
36	REBCO-2	44	31.5	1.4	12.1	12.51	26.5	10.6	2.5	60	2.3	87	38	17.9		
37	Rhemoura	51.9	38.6	1.3	11.95	12.2	32.3	22.6	1.4	30	1.4	83	60	17.8	1.62	1.79
38	Sepia	43.4	20.5	2.1	12.17	12.67	24.1	4.8	5	80	4.6	92	20	18.1	1.15	1.24
39	Sib. Light	41.9	27.1	1.5	12.14	12.53	25	10	2.5	60	2.3	78	34	17.6	1.75	1.91
40	SGC	52	37.6	1.4	12.1	12.41	26.6	14.6	1.8	45	1.7	90	52	18	1.32	1.46
41	Tartaruga	47.6	40.7	1.2	12.02	12.33	29.8	17.9	1.7	40	1.6	94	59	18.1	1.08	1.18
42	Tempa Rossa	71.1	59.6	1.2	11.63	12.04	44.7	29.1	1.5	35	1.5	113	75	18.7	0.89	1.04
43	Vald'Agri	42.6	25.5	1.7	11.99	12.47	30.9	12.4	2.5	60	2.2	69	31	17.3	2.40	2.76
44	Varandey	39.4	34.6	1.1	12.12	12.32	25.9	18.1	1.4	30	1.4	76	56	17.6	1.87	2.05
45	Western Desert	32.5	1	12.05	12.2	28.6					1.2	64	53	17.2	2.91	3.00
46	Es Sider	36.3	31	1.2	12.21	12.44	22.2	13.3	1.7	40	1.6	71	46	17.4	2.16	2.51
47	Payra Gold				11.94	12.7	32.8	3.3	10	90	9	91	10	18	1.15	1.23
48	KEBCO				12.04	12.42	28.9	14.4	2	50	1.9	86	46	17.9	1.46	1.56
	min	22.1	13.9	1	0.8	237	10.9	11.8	12.5	3.3	1	0	1	5.3	0.56	0.68
	max	93.5	59.6	2.2	1	558	12.5	12.7	74.7	37.3	10	90	9	137.4	4.79	4.83

Table 3. μ-values obtained from ICRA evaluation of parameters reported in Table 2.

μ	Sp	Sp cr.	RCI	Kw	Kw Blend	Sp (Mod.)	Sp cr. (Mod)	RCI (Mod.)	n-Heptane	SBN/IN	SBN	IN	δCO	CII(C7)	CII(C5)
Sp	1.00	0.78	0.43	0.22	0.29	0.75	0.68	0.42	0.42	0.44	0.75	0.65	0.73	0.24	0.27
Sp cr.	0.78	1.00	0.23	0.31	0.27	0.67	0.72	0.33	0.33	0.35	0.69	0.72	0.67	0.30	0.33
RCI	0.43	0.23	1.00	0.44	0.58	0.45	0.32	0.61	0.62	0.62	0.43	0.30	0.42	0.48	0.46
Kw	0.22	0.31	0.44	1.00	0.74	0.02	0.23	0.46	0.47	0.47	0.24	0.33	0.23	0.71	0.71
Kw blend	0.29	0.27	0.58	0.74	1.00	0.23	0.01	0.71	0.72	0.72	0.33	0.13	0.32	0.63	0.63
Sp (mod.)	0.75	0.67	0.45	0.02	0.23	1.00	0.74	0.43	0.43	0.45	0.71	0.63	0.69	0.25	0.26
Sp cr. (mod)	0.68	0.72	0.32	0.23	0.01	0.74	1.00	0.19	0.19	0.21	0.64	0.84	0.62	0.34	0.35
RCI (mod.)	0.42	0.33	0.61	0.46	0.71	0.43	0.19	1.00	0.99	0.97	0.45	0.13	0.44	0.42	0.41
n-Heptane	0.42	0.33	0.62	0.47	0.72	0.43	0.19	0.99	1.00	0.97	0.45	0.13	0.44	0.43	0.42
SBN/IN	0.44	0.35	0.62	0.47	0.72	0.45	0.21	0.97	0.97	1.00	0.48	0.15	0.47	0.41	0.41
SBN	0.75	0.69	0.43	0.24	0.33	0.71	0.64	0.45	0.45	0.48	1.00	0.66	0.96	0.06	0.08
IN	0.65	0.72	0.30	0.33	0.13	0.63	0.84	0.13	0.13	0.15	0.66	1.00	0.63	0.34	0.36
δCO	0.73	0.67	0.42	0.23	0.32	0.69	0.62	0.44	0.44	0.47	0.96	0.63	1.00	0.04	0.06
CII(C7)	0.24	0.30	0.48	0.71	0.63	0.25	0.34	0.42	0.43	0.41	0.06	0.34	0.04	1.00	0.96
CII(C5)	0.27	0.33	0.46	0.71	0.63	0.26	0.35	0.41	0.42	0.41	0.08	0.36	0.06	0.96	1.00

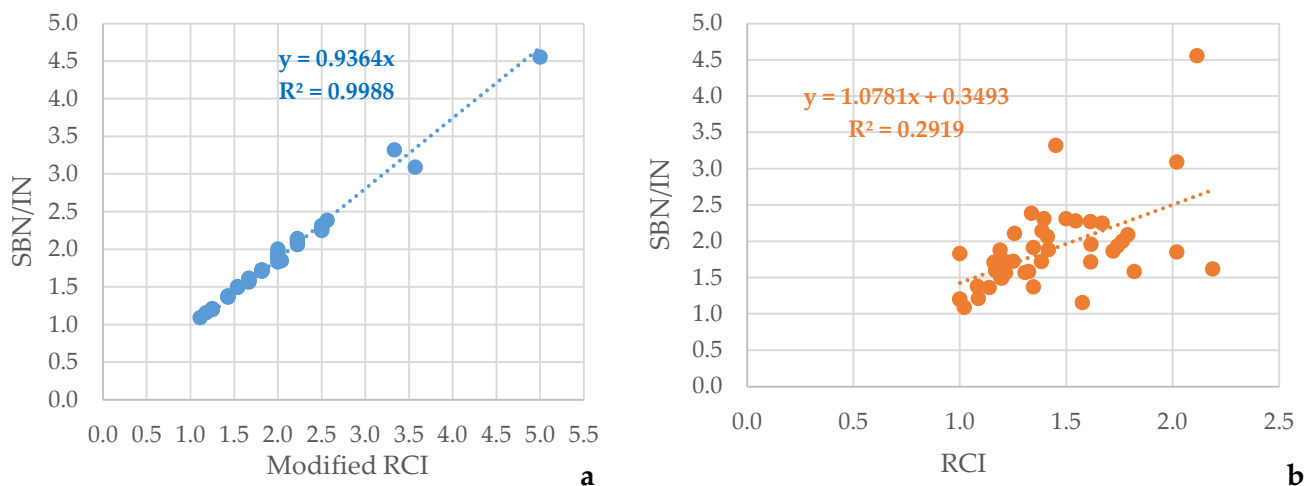
Note: Green color means statistically meaningful positive relation; red color implies statistically meaningful negative relation. The intensity of the color designates the strength of the relation. The higher the color intensity, the higher the strength of the relation. Yellow color denotes dissonance.

Table 4. ν -values obtained from ICrA evaluation of parameters reported in Table 2.

ν	Sp	Sp cr.	RCI	Kw	Kw Blend	Sp (Mod.)	Sp cr. (Mod.)	RCI (Mod.)	n-Heptane	SBN/IN	SBN	IN	δ CO	CII(C7)	CII(C5)
Sp	0.00	0.20	0.47	0.75	0.68	0.22	0.29	0.48	0.49	0.48	0.22	0.33	0.20	0.72	0.70
Sp cr.	0.20	0.00	0.68	0.67	0.71	0.30	0.27	0.58	0.59	0.58	0.29	0.26	0.27	0.68	0.65
RCI	0.47	0.68	0.00	0.46	0.32	0.44	0.58	0.23	0.23	0.24	0.46	0.61	0.45	0.42	0.43
Kw	0.75	0.67	0.46	0.00	0.23	0.97	0.74	0.43	0.43	0.45	0.71	0.63	0.69	0.25	0.26
Kw blend	0.68	0.71	0.32	0.23	0.00	0.73	0.99	0.19	0.19	0.20	0.64	0.85	0.62	0.34	0.35
Sp (mod.)	0.22	0.30	0.44	0.97	0.73	0.00	0.23	0.46	0.47	0.46	0.24	0.34	0.23	0.71	0.71
Sp cr. (mod.)	0.29	0.27	0.58	0.74	0.99	0.23	0.00	0.71	0.72	0.71	0.33	0.13	0.31	0.63	0.63
RCI (mod.)	0.48	0.58	0.23	0.43	0.19	0.46	0.71	0.00	0.00	0.00	0.44	0.77	0.42	0.48	0.49
n-Heptane	0.49	0.59	0.23	0.43	0.19	0.47	0.72	0.00	0.00	0.01	0.45	0.78	0.43	0.48	0.49
SBN/IN	0.48	0.58	0.24	0.45	0.20	0.46	0.71	0.00	0.01	0.00	0.43	0.77	0.41	0.50	0.51
SBN	0.22	0.29	0.46	0.71	0.64	0.24	0.33	0.44	0.45	0.43	0.00	0.31	0.00	0.91	0.88
IN	0.33	0.26	0.61	0.63	0.85	0.34	0.13	0.77	0.78	0.77	0.31	0.00	0.30	0.63	0.61
δ CO	0.20	0.27	0.45	0.69	0.62	0.23	0.31	0.42	0.43	0.41	0.00	0.30	0.00	0.89	0.87
CII(C7)	0.72	0.68	0.42	0.25	0.34	0.71	0.63	0.48	0.48	0.50	0.91	0.63	0.89	0.00	0.02
CII(C5)	0.70	0.65	0.43	0.26	0.35	0.71	0.63	0.49	0.49	0.51	0.88	0.61	0.87	0.02	0.00

Note: Green color means statistically meaningful positive relation; red color implies statistically meaningful negative relation. The intensity of the color designates the strength of the relation. The higher the color intensity, the higher the strength of the relation. Yellow color denotes dissonance.

As shown in the data of Tables 3 and 4, the original RCI does not have a statistically meaningful relation to both $\frac{S_{BN}}{I_N}$ and modified RCI, while the modified RCI and $\frac{S_{BN}}{I_N}$ have a strong positive consonance ($\mu = 0.94$; $\nu = 0.01$). The content of n-heptane at the onset of the asphaltene precipitation point has a strong positive consonance with both the modified RCI ($\mu = 1.00$; $\nu = 0.00$) and $\frac{S_{BN}}{I_N}$ ($\mu = 0.94$; $\nu = 0.01$), whereas the original RCI exhibits a lack of a statistical meaningful relation ($\mu = 0.68$; $\nu = 0.23$). Figure 2 exemplifies the good correlation of the modified RCI to $\frac{S_{BN}}{I_N}$ and the poor correlation of the RCI to $\frac{S_{BN}}{I_N}$.

**Figure 2.** Relation of modified RCI to $\frac{S_{BN}}{I_N}$ (a) and of RCI to $\frac{S_{BN}}{I_N}$ (b).

The data in Tables 3 and 4 also indicate that the colloidal instability indices CII(C5) and CII(C7) have a statistically meaningful strong negative consonance with the solubility blending number ($\mu = 0.06$; $\nu = 0.91$) and the crude oil solubility parameter δ CO ($\mu = 0.04$; $\nu = 0.89$). These findings imply that the solubility power of a crude oil increases with a reduction in the colloidal instability index, as displayed in Figure 3.

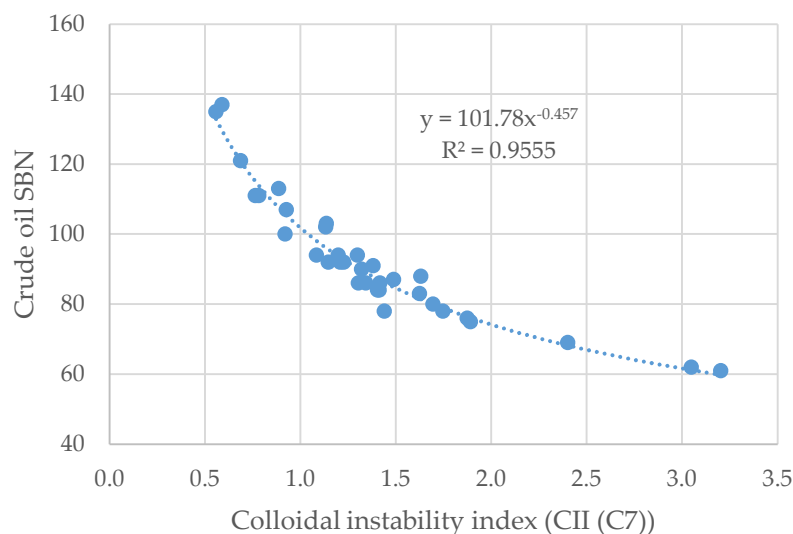


Figure 3. Relation of crude oil instability index to the petroleum solubility number.

Another testimony for the drawback of oil compatibility evaluation by using the original RCI was observed during the performance of the n-heptane dilution test, and HTSD analyses served as a basis for the calculation of the Sp and Sp critical for both samples of Helm crude oil. Figure 3 displays a graph of the dependence of the sediment content on the concentration of n-heptane in its mixtures with both Helm crude oil samples. The data in Figure 4 exhibit that the Helm 1.2024 sample needs a higher amount of n-heptane to be added to start asphaltene precipitation. Therefore, logically, this sample should report a lower Sp critical than that of the Helm 1.2022 sample. Referring to the data in Table 2, however, a higher Sp critical value is ascribed to Helm 1.2024 (Sp critical = 43 versus 30.2 of Helm 1.2022). The reason for this abnormal report obviously lies in the distillation characteristics of the Helm–heptane samples at the point of asphaltene precipitation measured by the high-temperature simulation distillation technique, as indicated in Table S1. Due to these distillation characteristics, the K_w -characterization factor of Helm 1.2022–heptane mixtures ($K_w = 11.94$) is higher than that of the blend Helm 1.2024–heptane mixtures ($K_w = 11.69$), which eventually leads to a higher calculated Sp critical value for the Helm 1.2024 sample.

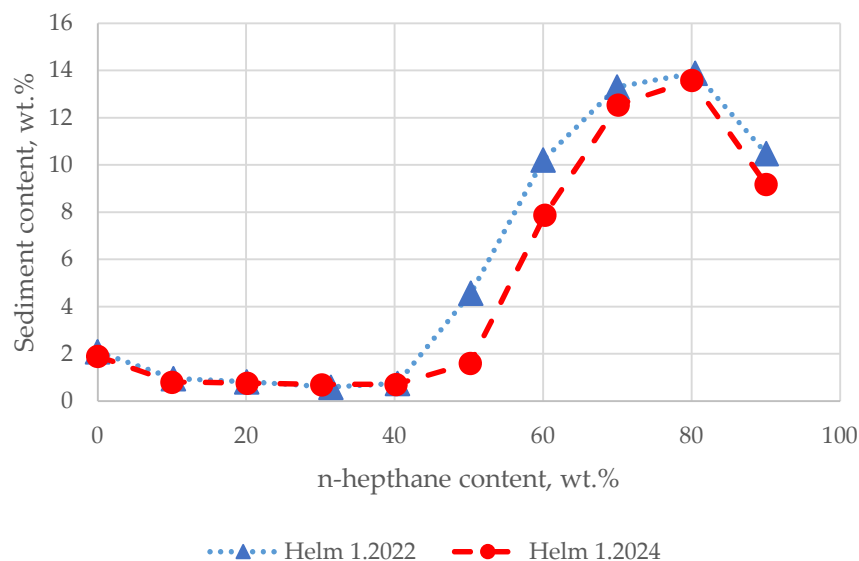


Figure 4. Sediment content dependence on n-heptane concentration in the mixtures with both Helm crude oil samples.

3.2. Crude Oil Properties and Compatibility Index Relations

Table S2 presents data of true boiling point (TBP) wide fraction yields of investigated crude oil samples. The range of the variation in the TBP wide fraction yields is relatively wide, as shown in Table 5.

Table 5. Scope of fluctuation of TBP fraction yields of studied crude oils.

TBP Wide Fraction Yields	IBP-110 °C, wt.%	110–180 °C, wt.%	180–240 °C, wt.%	240–360 °C, wt.%	360–540 °C, wt.%	>540 °C, wt.%
Min	1.2	1.9	2.5	12.8	18.5	5.2
Max	18.1	20.2	13.9	34.9	40.6	50.2

Tables 6 and 7 show the μ -values and ν -values of the intercriteria analysis evaluation of the data in Table S2 along with the data in Table 2.

Table 6. μ -values obtained from ICrA of parameters reported in Tables S2 and 2.

μ	IBP-110 °C, wt.%	110–180 °C, wt.%	180–240 °C, wt.%	240–360 °C, wt.%	360–540 °C, wt.%	>540 °C, wt.%	SP	SP cr (Modified)	RCI (Modified)
IBP-110 °C, wt.%	1.00	0.85	0.77	0.66	0.24	0.20	0.32	0.47	0.34
110–180 °C, wt.%	0.85	1.00	0.84	0.73	0.23	0.17	0.33	0.49	0.33
180–240 °C, wt.%	0.77	0.84	1.00	0.80	0.32	0.12	0.35	0.48	0.38
240–360 °C, wt.%	0.66	0.73	0.80	1.00	0.42	0.13	0.36	0.45	0.43
360–540 °C, wt.%	0.24	0.23	0.32	0.42	1.00	0.60	0.53	0.44	0.56
>540 °C, wt.%	0.20	0.17	0.12	0.13	0.60	1.00	0.66	0.53	0.55
SP	0.32	0.33	0.35	0.36	0.53	0.66	1.00	0.68	0.48
SP cr (modified)	0.47	0.49	0.48	0.45	0.44	0.53	0.68	1.00	0.18
RCI (modified)	0.34	0.33	0.38	0.43	0.56	0.55	0.48	0.18	1.00

Note: Green color means statistically meaningful positive relation; red color implies statistically meaningful negative relation. The intensity of the color designates the strength of the relation. The higher the color intensity, the higher the strength of the relation. Yellow color denotes dissonance.

Table 7. ν -values obtained from ICrA of parameters reported in Tables S2 and 2.

N	IBP-110 °C, wt.%	110–180 °C, wt.%	180–240 °C, wt.%	240–360 °C, wt.%	360–540 °C, wt.%	>540 °C, wt.%	SP	SP cr (Modified)	RCI (Modified)
IBP-110 °C, wt.%	0.00	0.12	0.21	0.31	0.73	0.77	0.65	0.50	0.58
110–180 °C, wt.%	0.12	0.00	0.14	0.24	0.74	0.81	0.64	0.48	0.59
180–240 °C, wt.%	0.21	0.14	0.00	0.17	0.65	0.85	0.61	0.49	0.53
240–360 °C, wt.%	0.31	0.24	0.17	0.00	0.54	0.84	0.59	0.52	0.48
360–540 °C, wt.%	0.73	0.74	0.65	0.54	0.00	0.38	0.42	0.53	0.36
>540 °C, wt.%	0.77	0.81	0.85	0.84	0.38	0.00	0.31	0.45	0.38
SP	0.65	0.64	0.61	0.59	0.42	0.31	0.00	0.28	0.43
SP cr (modified)	0.50	0.48	0.49	0.52	0.53	0.45	0.28	0.00	0.74
RCI (modified)	0.58	0.59	0.53	0.48	0.36	0.38	0.43	0.74	0.00

Note: Green color means statistically meaningful positive relation; red color implies statistically meaningful negative relation. The intensity of the color designates the strength of the relation. The higher the color intensity, the higher the strength of the relation. Yellow color denotes dissonance.

The data in Tables 6 and 7 indicate that the oil compatibility parameters S_p , S_p critical, and modified RCI have no statistically meaningful relation to any TBP fraction yield. It deserves noting here that the statistically meaningful negative consonances of the vacuum residue (>540 °C) fraction yield with the lighter fractions (light naphtha (IBP-110 °C); heavy naphtha (110–180 °C); kerosene (180–240 °C) and diesel (240–360 °C)) of the studied crude oils resemble those obtained during the hydrocracking of the vacuum residue, as shown in Tables S3 and S4. The same similarity is observed between relations of the K_w -characterization factor of different crude oil fractions and that of oil fractions obtained during vacuum residue hydrocracking (see Tables S5–S8). This similarity between

oil fraction relation to each other in both hydrocracking fraction yields and petroleum fraction yields supports the perception that petroleum has been formed by the cracking of higher-molecular-weight organic matter, known as kerogen, accumulated in the Earth's bowels [82–86]. It should be noted here that the ICRA evaluation of vacuum residue hydrocracking data shown in Tables S3 and S4 is related to the hydrocracking of a vacuum residue derived from a single crude oil. However, when the data of the hydrocracking of 13 vacuum residues obtained from 13 crude oils are evaluated by ICRA, as indicated in Tables S9 and S10, the consonances of unconverted vacuum residue and the lighter oil fractions, although statistically meaningful, are weaker than those observed from the hydrocracking data of the single vacuum residue (see Tables S3 and S4), and they are very close to those observed at the petroleum fractions (see Tables 6 and 7). This is in line with the different classifications of petroleum origin coming from the diverse kerogen types [89–102], showing that the various kerogens can provide different conversion levels and different selectivities [92]. Similar to the different colloidal stabilities of the n-heptane insoluble fraction of the unconverted hydrocracked vacuum residues obtained from diverse crude oils [11,73,103], the colloidal stability of the n-heptane insoluble fraction of the various crude oils can also be different [43,44]. Thus, one may expect that the crude oils formed from distinct kerogen types may have different stabilities of their n-heptane insoluble fraction. Another factor that can influence the oil colloidal stability in both crude oil and vacuum residue hydrocracked synthetic crude oil is the maturity/conversion levels. The higher the conversion of the vacuum residue hydrocracking is, the lower the colloidal stability of the hydrocracked n-heptane insoluble fraction is, and the lighter the synthetic crude oil is [11,16]. The same seems to be valid for the crude oils characterized by a high degree of maturity, which have experienced a higher extent of cracking reactions in the Earth's bowels. They are lighter, with a high content of light oil fractions which make the residual oil fraction less soluble and therefore less colloidal stable. The extra light crude oil CPC and the light crude oil Western Desert, which are good examples of high-maturity crude oils, whose stability was not possible to determine by the n-heptane dilution test (see Table 2) probably because of their low asphaltene content, by using a spot test, they are certainly classified as unstable (see Figure 5).

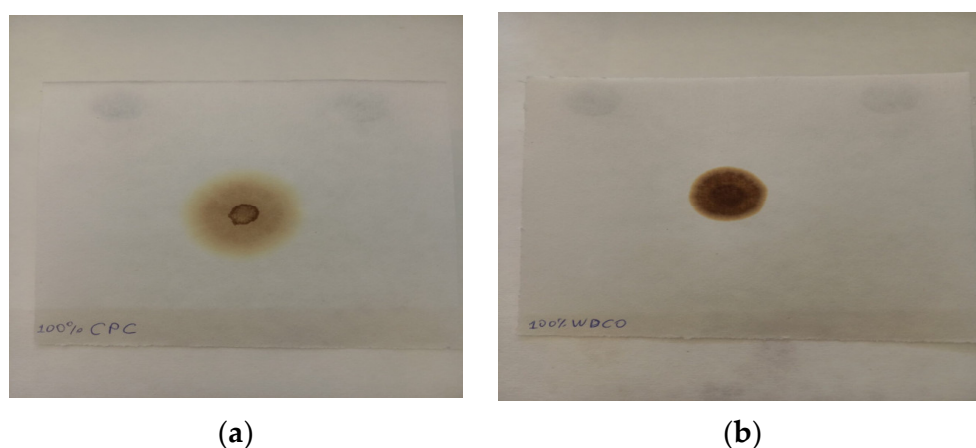


Figure 5. Spot test result of CPC crude oil (a) and Western Desert crude oil (b).

On the one hand, this can explain why the lighter crude oils are more prone to form sediments than the heavier petroleum oils [14–17], and on the other hand, this result suggests that the oil colloidal stability is governed not only by the n-heptane insoluble fraction characteristics but also by the characteristics of n-heptane soluble oil fraction.

The n-heptane insoluble fraction of the different crude oils has been formed as a result of kerogen cracking [104], and its properties can be considered to be a function of both pristine kerogen properties and the extent of its conversion.

The bulk properties of the studied crude oils and some characteristics of their vacuum residue fractions shown in Table S11, along with the data from Table 2, were evaluated by ICrA. The μ - and ν -values from the ICrA evaluation are presented in Tables S12 and S13. The data in Tables S12 and S13 indicate that the S_p critical does not have any statistically meaningful relation to any of the studied crude oil properties.

A regression analysis of the crude oil data and S_p critical was performed, and it was found that three crude oil properties, density, vacuum residue fraction density, and TBP T50 wt.% point, can be used to predict the S_p cr. Considering that the necessary condition for linear regression is that the statistical distribution of the dependent and independent variables should be normal, the four variables S_p cr. (dependent variable), and density, vacuum residue fraction density, and TBP T50 wt.% point (independent variables), were evaluated for their proximity to normal distribution, where the distribution deviates from the normal transformations like x^n , e^x , $\ln(x)$, etc. [105]. Figures S1–S4 display histograms of the distribution of the four variables and the transformations applied to make the variable distribution closer to the normal one. After these transformations, the following regression was derived to predict the crude oil S_p cr. from the crude oil density, vacuum residue fraction density, and TBP T50 wt.% point.

$$S_{p\ cr.} = \left[-16.6768 + 21.12136 \times CO_{D15} + 4.616382 \times VR_{D15}^2 - 1.9 \times 10^{-5} \times T_{50}^2 \right]^2 \rightarrow R = 0.80, \text{relativestandarddeviation} = 4.3\%. \quad (13)$$

where

CO_{D15} = density of crude oil at 15 °C, g/cm³;

VR_{D15} = density of vacuum residue fraction of crude oil at 15 °C, g/cm³;

T_{50} = true boiling point temperature at 50% evaporation of crude oil. °C.

Having in mind that the artificial neural network (ANN) approach to model different oil properties reported a higher accuracy of prediction than that of the regression methods [106–113], we decided to develop an ANN model to predict the S_p critical of petroleum fluids. For this purpose, we used more data than those listed in Table 2 and collected data on 110 crude oils and residues from the literature [34,42–44], as well as some additional unpublished data of our own. The range of the variation in the oil properties used to model the S_p critical by ANN is summarized in Table 8.

Table 8. Oil input data for ANN modeling of S_p critical.

Range	SG	Sat	Aro	Res	n-C ₇ asp.	n-C ₅ asp.	Tb	T10	T30	T50	T70	T90	Kw	S_p Critical
min	0.773	6.0	7.1	1.4	0.0	1.8	196	98	174	187	193	245	10.6	3.3
max	1.111	91.1	69.2	11.1	36.6	47.7	659	429	639	667	700	984	12.6	62.9

For the development of the artificial neural network model, a three-layer deep learning neural network with a structure of 13 inputs and 132 neurons in the first layer, 42 in the second layer, 16 in the third layer, 10 in the fourth layer, 8 in the fifth layer, and 1 in the output layer was used. Figure 6 presents the basic parameters of the neural network. The entire training process took 15 iterations, and the performance was 0.057555. The training process is shown in Figure 7. The regression coefficients of the artificial neural network are as follows: training—0.79082, testing—0.90587, validation—0.63821, all—0.79535 (Figure 8).

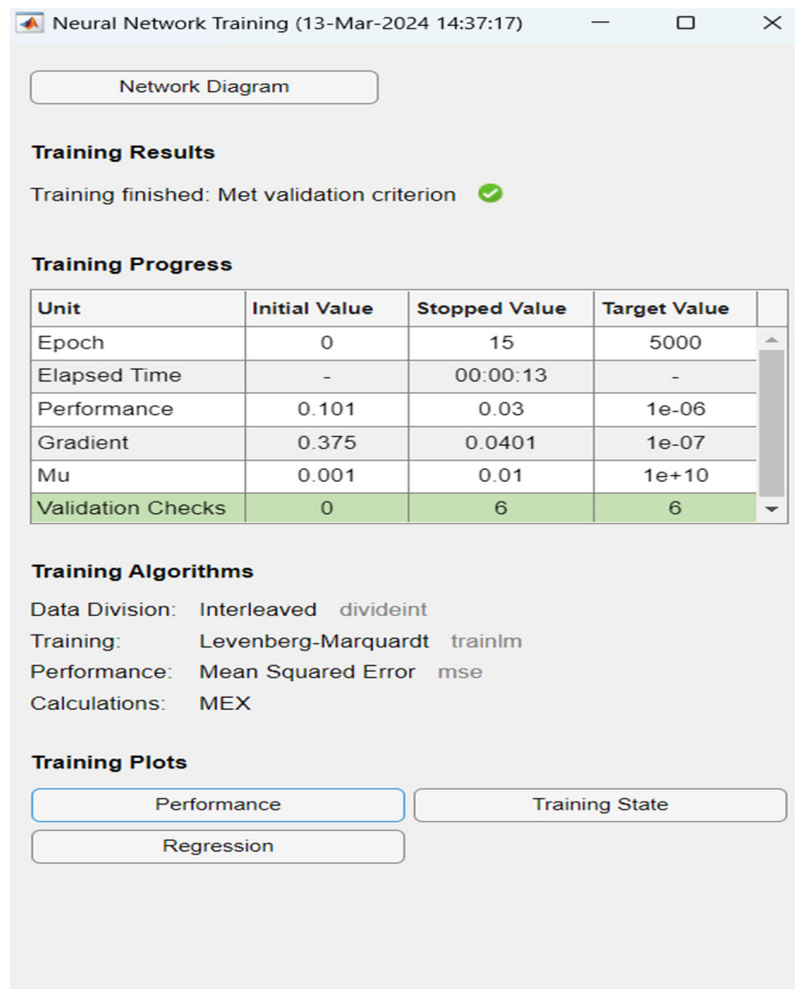


Figure 6. Structure of the neural network employed in this study.

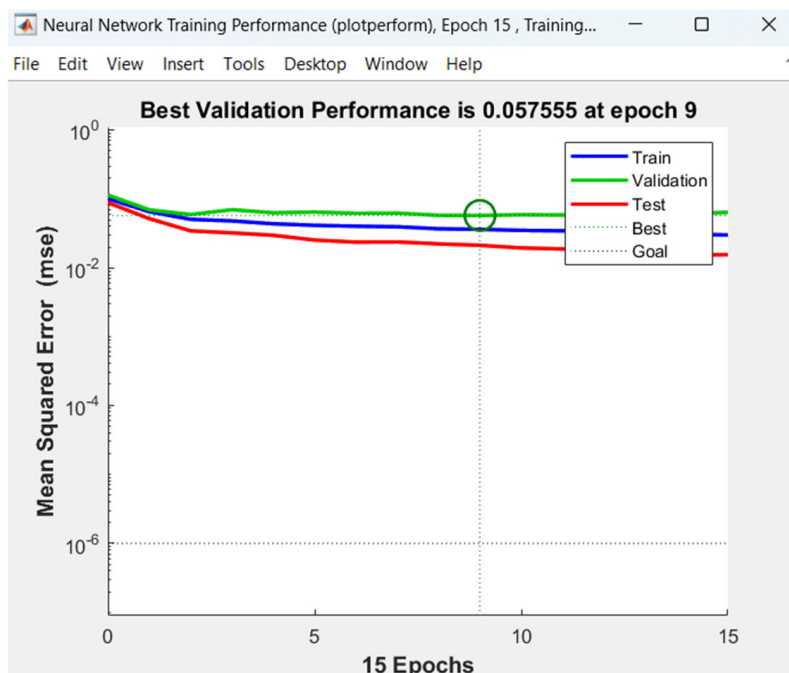


Figure 7. Training process of the neural network.

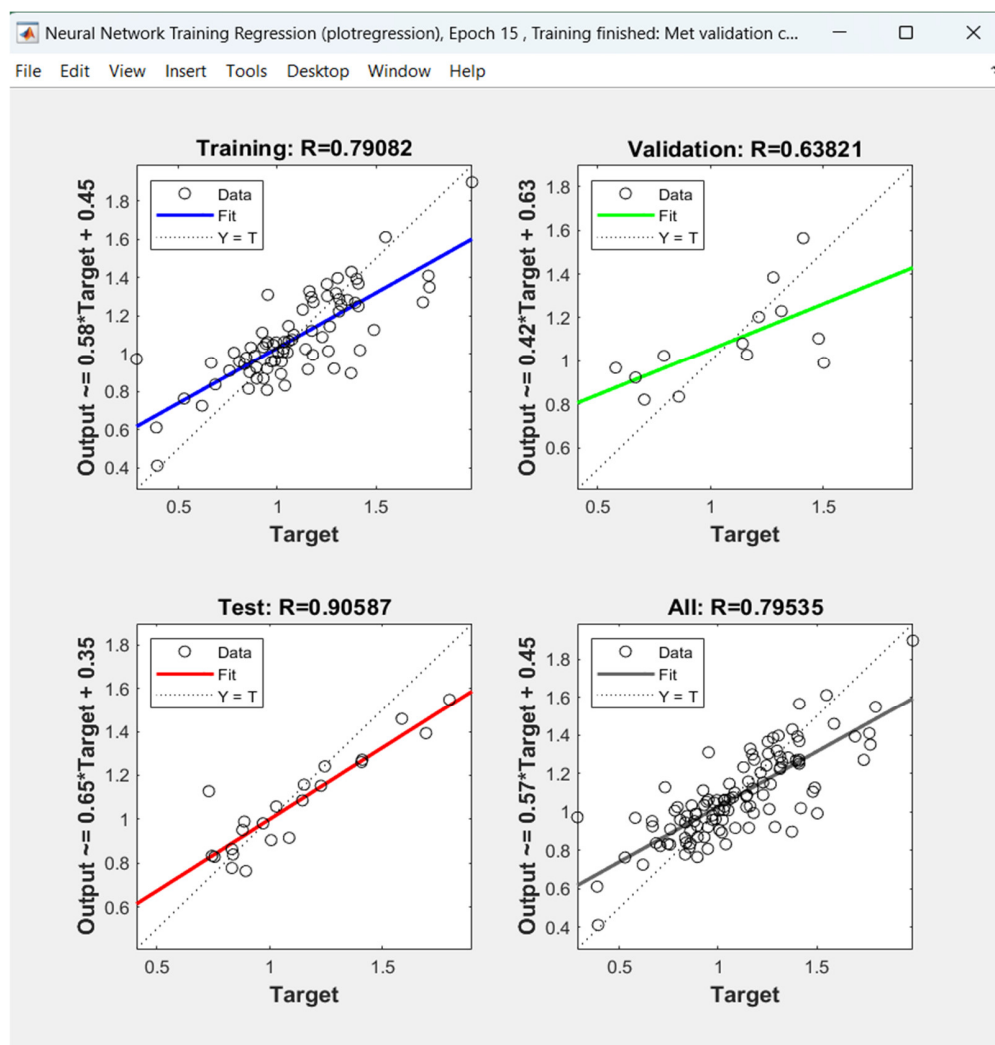


Figure 8. Regression coefficients of the learning process of the ANN.

For the investigated 48 crude oil samples in this study, the ANN model predicts the S_p critical with $R = 0.799$ and a relative standard deviation of 4.6%, which is almost the same as that of the regression in Equation (13). This accuracy of prediction is somewhat better than that announced by Ali et al. [66], who forecasted asphaltene stability by other metaheuristic methods (various machine learning algorithms). The accuracy of the regression and ANN models developed in this work suggests that the available model input oil properties, similar to the SARA information used by Ali et al. [67], are not sufficiently capable of predicting very accurately the oil stability expressed by the S_p critical.

The crude oils which, after mixing with n-heptane, did not show any sign of flocculation (see Figure 1a–c and Table 2) cannot be assessed for their compatibility with the other crude oils because the S_p critical cannot be determined. In these cases, in order to understand whether the blending of these crudes with other petroleum oils can lead to sediment formation, it is necessary to perform a compatibility test where instead of n-heptane being used as an anti-solvent, these crude oils are used. The results of such compatibility tests carried out with the Kirkuk imported atmospheric residue with CPC, Western Desert (WDCO), and n-heptane (for comparison reasons) are depicted in Figure 9.

The data in Figure 9 indicate that the flocculation with the three diluents n-heptane, CPC crude oil, and WDCO starts at 50% content in their blend with the Kirkuk AR. However, the trend of sediment increment with the three diluents is different. While the n-heptane, as expected, increases sharply, the sediment content in Kirkuk AR is at 50% n-heptane content, and then the sediment content does not go up significantly, meaning that the addition of

CPC crude oil exponentially augments the sediment content, reaching the highest value among the three diluents. The WDCO addition to the Kirkuk AR demonstrates the lowest sediment content increment. These data suggest that the concept of the RCI is not applicable to oils whose S_p critical cannot be determined. Moreover, the sediment formation potential seems to be different for the diverse diluents exhibiting an extremely high sediment raise for the blend CPC–Kirkuk AR when the CPC content is higher than 70%. Such a compatibility test is recommended to be performed before making a decision to process a blend of light crude oils and heavier oils in order to improve profitability. Such an opportunity may look attractive for European refiners who have processed lighter crude oils lately [114].

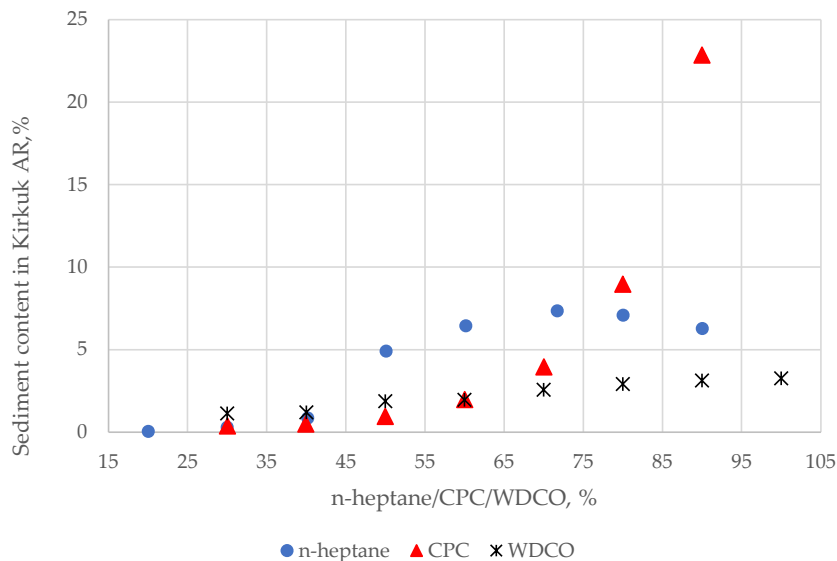


Figure 9. Kirkuk atmospheric residue sediment content relation to content of n-heptane, CPC crude oil, and Western Desert crude oil (WDCO).

The modified RCI crude mixture, containing 13 of the investigated petroleum oils, was juxtaposed against the desalting efficiency of the LUKOIL Neftohim Burgas refinery crude distillation unit, as it is known that the lower compatibility [65,115,116] of processed crude oil is related to a lower desalting efficiency, as shown in Figure 10.

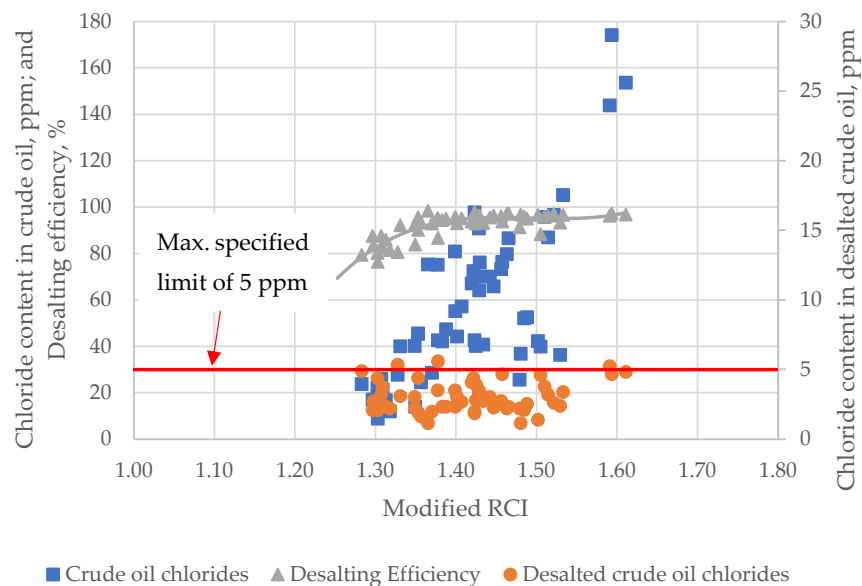


Figure 10. Modified RCI crude blend against desalting efficiency.

The data in Figure 10 indicate that lowering the modified RCI is associated with desalting efficiency deterioration. The data in Figure 9 also suggest that when the RCI is below 1.3, a significant drop in crude desalting efficiency can be expected. Although the minimum desalting efficiency in this study was 77%, the maximum specified limit of 5 ppm (1.5 PTB (pounds of salt per thousand barrels of oil)) was almost not achieved (only three cases with 5.3, 5.4, and 5.6 ppm of salt in desalted crude oil). A decrease in the modified RCI below 1.3, however, could be considered undesirable because of the expected deterioration of the crude oil's desalting efficiency.

The formation of petroleum is quite a complex process in which the different types of kerogens are cracked in the Earth's bowels for a different period of time in a distinct environment that eventually leads to petroleum oils with a highly diverse composition and properties. Petroleum researchers have concluded that no two crude oils are the same [117–119]. In this work, all of the 41 studied individual crude oils were evaluated for their similarity on the basis of boiling point distribution, density, and sulfur distributions, information extracted from crude oil assays. The maximum positive consonance achieved for this crude oil dataset was 0.933 for the crude oils of Basrah Light and Basrah Med. (Tables S14 and S15), which is below 0.95, above which it is deemed that the similarity is strong, supporting the statements made above that no two crude oils are the same. Even for the crude oils which have a relatively high consonance such as Vald'Agri and Kirkuk ($\mu = 0.914$; $\nu = 0.079$), the stability parameters of the modified RCI (2.5 and 1.3, respectively) and Sp critical (12.4 and 23.0, respectively) are too different. This suggests that the prediction of the colloidal stability parameters of the individual crude oils would be very difficult, as was already shown earlier in this research. The experimental determination of the colloidal stability parameters seems to remain the most reliable tool to determine the compatibility of any crude oil mixture.

4. Conclusions

After investigating 48 crude oil samples by performing true boiling point (TBP) analysis, high-temperature simulation distillation, SARA analysis, viscosity, density and sulfur distribution of narrow petroleum fractions, vacuum residue characterization (SARA, density, Conradson carbon, asphaltene density), and an n-heptane dilution test by centrifugation, the following conclusions were made.

1. The determination of the Sp critical by the original method of Nemana calculating the Kw-characterization factor by using the distillation characteristics of the mixture crude oil–n-heptane at the onset of asphaltene precipitation may report inconsistent results. Thus, the modification of Nemana's method is proposed that calculates the Kw-characterization of the blend crude oil–n-heptane at the onset of asphaltene flocculation as a sum of the crude oil Kw factor multiplied by its weight part at the point of asphaltene onset precipitation, and the Kw factor of n-heptane multiplied by its weight part in the admixture.
2. The $\frac{S_{BN}}{I_N}$ ratio strongly correlates with the modified relative stability index with a squared correlation coefficient of $R^2 = 0.9873$, while with the original RCI of Nemana, it does not correlate well ($R^2 = 0.2919$).
3. By employing intercriteria analysis, it was found that the crude oil characteristics involved in a crude assay do not exhibit any statistically meaningful relation to the compatibility indices determined by using the n-heptane dilution test. The Kw-factor of the vacuum residue fraction of the crude oils that is determined on the basis of the density and high-temperature simulated distillation of the vacuum residue demonstrates a negative consonance ($\mu = 0.24$; $\nu = 0.74$) with the insolubility number, which is very close to the threshold of ICRA defined for statistically meaningful negative consonance ($\mu = 0.25$; $\nu = 0.75$). This finding is in line with our earlier research, indicating that the higher the aromaticity of the vacuum residue, the higher the insolubility number of its asphaltene fraction [12].

4. By using regression analysis of the data generated in this work, a correlation was developed that shows that the Sp critical increases with the enhancement of the vacuum residue fraction's density, crude oil density augmentation, and crude oil T50% reduction. This correlation confirms the earlier statement that the higher the vacuum residue aromaticity (density, Conradson carbon content), the lower its asphaltene fraction solubility.
5. Artificial neural network modeling was also applied in this work. The ANN model of the Sp critical, however, in contrast to the reports in other studies modeling other petroleum properties by ANN, did not show a better prediction ability than that of the regression model.
6. The ICrA evaluation of the petroleum properties and those of the products obtained by vacuum residue hydrocracking, whose conversion is thermal, showed a clear similarity between both, which supports the perception that the petroleum was formed by thermal cracking in the Earth's bowels.
7. A future study directed toward searching for the link between kerogen type and maturity of a crude oil may improve the accuracy of the prediction of oil compatibility indices.
8. It was found that the efficiency of crude oil desalting starts to decline when the modified RCI drops below 1.4, confirming Wiehe's conclusion that the ratio $\frac{S_{BN}}{I_N}$, or its equivalent modified RCI, should be kept no lower than 1.4 to avoid any fouling or other incompatibility issues [4].

The crude oils whose asphaltene onset precipitation point cannot be determined by the n-heptane dilution test can be used as diluents instead of n-heptane in a centrifugation test to define the concentration at which flocculation start when they are mixed with other crude oils. The diverse crude oils whose oil compatibility indices cannot be determined by n-heptane dilution test crude oils may exhibit a different pattern in terms of sediment formation when blended with heavier oils, even worse than that observed with n-heptane. Such an example is the CPC crude oil when blended with an imported atmospheric residue from Kirkuk crude oil.

Supplementary Materials: The following supporting information can be downloaded at: <https://www.mdpi.com/article/10.3390/pr12040780/s1>, Figure S1: Histogram of vacuum residue fraction density (a) and that of vacuum residue density (b); Figure S2: Histogram of crude oil density; Figure S3: Histogram of crude oil T50% (a) and that of T50%2 (b); Figure S4: Histogram of crude oil Sp critical (a) and that of Sp critical 0.5 (b); Table S1: Data of HTSD and density of both samples of crude oil Helm and their mixtures with n-heptane at the point of asphaltene precipitation onset, along with Kw-characterization factor, Sp , and Sp critical; Table S2: True boiling point wide fraction yields of investigated crude oil samples; Table S3: μ -values obtained from ICrA evaluation of fraction yields obtained during vacuum residue hydrocracking (vacuum residue hydrocracking data taken from Ref. [66]. These data are related to a single crude oil source); Table S4: ν -values obtained from ICrA evaluation of fraction yields obtained during vacuum residue hydrocracking (vacuum residue hydrocracking data taken from Ref. [66]. These data are related to a single crude oil source); Table S5: μ -values obtained from ICrA evaluation of Kw-characterization factors of crude oil fractions; Table S6: ν -values obtained from ICrA evaluation of Kw-characterization factors of crude oil fractions; Table S7: μ -values obtained from ICrA evaluation of Kw-characterization factors of vacuum residue hydrocracking fractions (data taken from Ref. [66]); Table S8: ν -values obtained from ICrA evaluation of Kw-characterization factors of vacuum residue hydrocracking fractions (data taken from Ref. [66]); Table S9: μ -values obtained from ICrA evaluation of fraction yields obtained during hydrocracking of vacuum residues originated from 13 crude oils; Table S10: ν -values obtained from ICrA evaluation of fraction yields obtained during hydrocracking of vacuum residues originated from 13 crude oils; Table S11: Bulk properties of studied crude oils and some characteristics of their vacuum residue fractions. Table S12: μ -values obtained from ICrA evaluation of crude bulk properties and some characteristics of their vacuum residue fractions and oil compatibility parameters; Table S13: ν -values obtained from ICrA evaluation of crude bulk properties and some characteristics of their vacuum residue fractions and oil compatibility parameters; Table S14: μ -values obtained from ICrA evaluation

for similarity of investigated 41 crude oils; Table S15. ν -values obtained from ICRA evaluation for similarity of investigated 41 crude oils.

Author Contributions: Conceptualization, D.S. and I.S.; methodology, M.T.; software, S.S. and S.R.; validation, F.v.d.B., A.N. and R.D.; formal analysis, I.K.; investigation, R.N., G.G. and A.V.; resources, D.S.; data curation, K.A.; writing—original draft preparation, D.S. and I.S.; writing—review and editing, D.S.; visualization, I.K.; supervision, D.S.; project administration, D.S. All authors have read and agreed to the published version of the manuscript.

Funding: This research received no external funding.

Data Availability Statement: Data are contained within the article.

Conflicts of Interest: Authors Ivelina Shiskova, Dicho Stratiev, Mariana Tavlieva, Angel Nedelchev, Rosen Dinkov, Iliyan Kolev, Georgi Georgiev were employed by LUKOIL Neftohim Burgas. Author Frans van den Berg was employed by Black Oil Solutions. The remaining authors declare that the research was conducted in the absence of any commercial or financial relationships that could be construed as a potential conflict of interest.

Nomenclature

A	Aromatics content
ANN	Artificial neural network
AR	Atmospheric residue
Aro	Aromatics
Asph	Asphaltenes
C5-asp	Content of asphaltenes insoluble in n-pentane, wt.%
C7-asp	Content of asphaltenes insoluble in n-heptane, wt.%
CII	Colloidal instability index
CII (C5)	Colloidal instability index based on C5 asphaltene content
CII (C7)	Colloidal instability index based on C7 asphaltene content
CO	Crude oil
CSI	Colloidal stability index
D15	Density at 15 °C, g/cm ³
DBASE	Density based asphaltene stability envelope
HD	Heptane dilution
HTSD	High-temperature simulant distillation
IBP	Initial boiling point
ICrA	Intercriteria analysis
I _N	Insolubility index
JM	Jamaluddin method
K _{co}	Characterization factor of crude oil
K _{hp}	Characterization factor of n-heptane
K _t	Characterization factor of toluene
K _w	Watson characterization factor
MJM	Modified Jamaluddin method
ND	Not determined
P	Heithaus parameter
PTB	Pounds of salt per thousand barrels of oil
QQA	Qualitative–quantitative analysis
RCI	Relative compatibility index
Res	Resins
SARA	Saturates, aromatics, resins, asphaltenes
Sat	Saturates
S _{BN}	Solubility blending number
SCP	Stability cross plot
SG	Specific gravity
SI	Stability index
SN	Separability number
SP	Stankiewicz plot
Sp	Solvent power

S_p blend	Solvent power of petroleum blend
S_p critical	Critical solvent power
T_{10}	Boiling point of evaporate at 10%, °C
T_{30}	Boiling point of evaporate at 30%, °C
T_{50}	Boiling point of evaporate at 50%, °C
T_{50}	Boiling point of evaporate at 50%, °C
T_{70}	Boiling point of evaporate at 70%, °C
T_{90}	Boiling point of evaporate at 90%, °C
TBP	True boiling point
TBP yield (>540 °C)	Yield of TBP fraction >540 °C, wt.%;
TBP yield (110–180 °C)	Yield of TBP fraction 110–180 °C, wt.%;
TBP yield (180–240 °C)	Yield of TBP fraction 180–240 °C, wt.%;
TBP yield (360–540 °C)	Yield of TBP fraction 360–540 °C, wt.%;
TBP yield (IBP–110 °C)	Yield of TBP fraction IBP–110 °C, wt.%;
TBP yield (IBP–360 °C)	Yield of TBP fraction IBP–360 °C, wt.%;
TE	Toluene equivalence
WDCO	Western Desert crude oil
δ_{CO}	Solubility parameter values of crude oil
μ	Positive consonance
ν	Negative consonance
X_i	Weight fraction of i component

References

- Wiehe, I.A.; Kennedy, R.J. Oil compatibility model and crude oil incompatibility. *Energy Fuels* **2000**, *14*, 56–59. [[CrossRef](#)]
- Wiehe, I.A.; Kennedy, R. Application of the oil compatibility model to refinery streams. *Energy Fuels* **2000**, *14*, 60–63. [[CrossRef](#)]
- Wiehe, I.A. *Process Chemistry of Petroleum Macromolecules*, 1st ed.; Taylor & Francis Group, CRC Press: Boca Raton, FL, USA, 2008.
- Wiehe, I.A.; Kennedy, R.; Dickakian, G. Fouling of nearly incompatible oils. *Energy Fuels* **2001**, *15*, 1057–1058. [[CrossRef](#)]
- Wiehe, I.A. Asphaltene solubility and fluid compatibility. *Energy Fuels* **2012**, *26*, 4004–4016. [[CrossRef](#)]
- Wiehe, I.A. Self-incompatible crude oils and converted petroleum resids. *J. Dispers. Sci. Technol.* **2004**, *25*, 333–339. [[CrossRef](#)]
- ASTM D7112; Standard Test Method for Determining Stability and Compatibility of Heavy Fuel Oils and Crude Oils by Heavy Fuel Oil Stability Analyzer (Optical Detection). ASTM International: West Conshohocken, PA, USA, 2019; Volume 05.03.
- ASTM D7157-22e1; Standard Test Method for Determination of Intrinsic Stability of Asphaltene-Containing Residues, Heavy Fuel Oils, and Crude Oils (n-Heptane Phase Separation; Optical Detection). ASTM International: West Conshohocken, PA, USA, 2022; Volume 05.03.
- ASTM D7061-19e1; Standard Test Method for Measuring n-Heptane Induced Phase Separation of Asphaltene-Containing Heavy Fuel Oils as Separability Number by an Optical Scanning Device. ASTM International: West Conshohocken, PA, USA, 2019; Volume 05.03.
- Van den Berg, F.G.A. History and Review of Dual Solvent Titration Methods. *Energy Fuels* **2022**, *36*, 8639–8648. [[CrossRef](#)]
- Mitkova, M.; Stratiev, D.; Shishkova, I.; Dobrev, D. *Thermal and Thermo-Catalytic Processes for Heavy Oil Conversion*; Professor Marin Drinov Publishing House of Bulgarian Academy of Sciences: Veliko Tarnovo, Bulgaria, 2017; Volume 13.
- Stratiev, D.; Shishkova, I.; Nedelchev, A.; Kirilov, K.; Nikolaychuk, E.; Ivanov, A.; Sharafutdinov, I.; Veli, A.; Mitkova, M.; Tsaneva, T.; et al. Investigation of relationships between petroleum properties and their impact on crude oil compatibility. *Energy Fuels* **2015**, *29*, 7836–7854. [[CrossRef](#)]
- Rogel, E.; Hench, K.; Miao, T.; Lee, E.; Dickakian, G. Evaluation of the compatibility of crude oil blends and its impact on fouling. *Energy Fuels* **2018**, *32*, 9233–9242. [[CrossRef](#)]
- Xiong, R.; Guo, J.; Kiyangi, W.; Feng, H.; Sun, T.; Yang, X.; Li, Q. Method for judging the stability of asphaltenes in crude oil. *ACS Omega* **2020**, *5*, 21420–21427. [[CrossRef](#)]
- Alimohammadi, S.; Zendejboudi, S.; James, L. A Comprehensive review of asphaltene deposition in petroleum reservoirs: Theory, challenges, and tips. *Fuel* **2019**, *252*, 753–791. [[CrossRef](#)]
- Izadpanahi, A.; Azin, R.; Osfouri, S.; Malakooti, R. Modeling of asphaltene precipitation in a light oil reservoir with high producing GOR: Case study. *Adv. Nano. Energy* **2019**, *3*, 270–279.
- Savage, G.; Sawhney, K. Light tight oil crude unit fouling root causes and troubleshooting. *PTQ Shale* **2015**, *2015*, 19–22.
- Ashoori, S.; Sharifi, M.; Masoumi, M.; Mohammad Salehi, M. The relationship between SARA fractions and crude oil stability. *Egypt. J. Pet.* **2017**, *26*, 209–213. [[CrossRef](#)]
- Sulaimon, A.A.; De Castro, J.K.M.; Vatsa, S. New correlations and deposition envelopes for predicting asphaltene stability in crude oils. *J. Pet. Sci. Eng.* **2020**, *190*, 106782. [[CrossRef](#)]
- Hascakir, B. A New approach to determine asphaltenes stability. In Proceedings of the SPE Annual Technical Conference and Exhibition, San Antonio, TX, USA, 9–10 October 2017.

21. Kumar, R.; Voolapalli, R.K.; Upadhyayula, S. Prediction of crude oil blends compatibility and blend optimization for increasing heavy oil processing. *Fuel Process. Technol.* **2018**, *177*, 309–327. [[CrossRef](#)]
22. Likhatsky, V.V.; Syunyaev, R.Z. New colloidal stability index for crude oils based on polarity of crude oil components. *Energy Fuels* **2010**, *24*, 6483–6488. [[CrossRef](#)]
23. Jamaluddin, A.K.M.; Nazarko, T.W.; Sills, S.; Fuhr, B.J. Deasphalted Oil: A natural asphaltene solvent. *SPE Prod. Facil.* **1996**, *11*, 161–165. [[CrossRef](#)]
24. Stankiewicz, A.; Flannery, M.D.; Fuex, N.A.; Broze, J.G.; Coach, J.L.; Dubey, S.T.; Leitko, A.D.; Nimmons, J.F.; Iyer, S.D.; Ratulowski, J. Prediction of asphaltene deposition risk in E&P operations. In Proceedings of the International Conference on Petroleum Phase Behavior and Fouling, New Orleans, LA, USA, 10–14 March 2002; pp. 410–416.
25. Gaona, J.A.S.; Manrique, J.P.B.; Majé, Y.M. Stability prediction for asphaltenes using SARA analysis for pure petroleum. *Ing. Y Reg.* **2010**, *7*, 103–110.
26. Guzmán, R.; Ancheyta, J.; Trejo, F.; Rodríguez, S. Methods for determining asphaltene stability in crude oils. *Fuel* **2017**, *188*, 530–543. [[CrossRef](#)]
27. Rathore, V.; Brahma, R.; Thorat, T.S.; Rao, P.V.C.; Choudary, N.V. Assessment of crude oil blends. *PTQ* **2011**, *Q4*, 1–6.
28. Mahmoud, M.B.; Aboujadeed, A.A. Compatibility assessment of crude oil blends using different methods. *Chem. Eng. Trans.* **2017**, *57*, 1705–1710.
29. Anderson, R.P.; Reynolds, J.W. *Methods for Assessing the Stability and Compatibility of Residual Fuel Oils*; National Institute for Petroleum and Energy Research, Bartlesville: Bartlesville, OK, USA, 1989.
30. Moura, L.G.M.; Santos, M.F.P.; Zilio, E.L.; Rolemberg, M.P.; Ramos, A.C.S. Evaluation of indices and of models applied to the prediction of the stability of crude oils. *J. Pet. Sci. Eng.* **2010**, *74*, 77–87. [[CrossRef](#)]
31. Kass, M.D.; Armstrong, B.L.; Kaul, B.C.; Connatser, R.M.; Lewis, S.; Keiser, J.R.; Jun, J.; Warrington, G.; Sulejmanovic, D. Stability, combustion, and compatibility of high-viscosity heavy fuel oil blends with a fast pyrolysis bio-oil. *Energy Fuels* **2020**, *34*, 8403–8413. [[CrossRef](#)]
32. Vráblík, A.; Schlehöfer, D.; Dlasková Jaklová, K.; Hidalgo Herrador, J.M.; Černý, R. Comparative study of light cycle oil and naphthalene as an adequate additive to improve the stability of marine fuels. *ACS Omega* **2022**, *7*, 2127–2136. [[CrossRef](#)]
33. Vráblík, A.; Hidalgo-Herrador, J.M.; Černý, R. RGB Histograms as a reliable tool for the evaluation of fuel oils stability. *Fuel* **2018**, *216*, 16–22. [[CrossRef](#)]
34. Ancheyta, J. Relative compatibility index for evaluation of the compatibility of crude oil blends. *Geoenergy Sci. Eng.* **2023**, *230*, 212246. [[CrossRef](#)]
35. Yadykova, A.Y.; Ilyin, S.O. Compatibility and rheology of bio-oil blends with light and heavy crude oils. *Fuel* **2022**, *314*, 122761. [[CrossRef](#)]
36. Odhiambo, J.O.; HaiJun, W.; Munyalo, J.M.; Fengguang, J. The use of separability number and SARA fractionation in studying asphaltenes stability in residual fuel oil. In Proceedings of the Sustainable Research and Innovation (SRI) Conference, Nairobi, Kenya, 6 May 2015; pp. 281–287.
37. Son, J.-M.; Kim, N.-K.; Shin, J.; Yang, Y.; Kim, Y.-W. Dispersing properties of heavy crude oil according to dispersant structures. *J. Korean Soc. Tribol. Lubr. Eng.* **2015**, *31*, 251–257.
38. Saboor, A.; Yousaf, N.; Haneef, J.; Ali, S.I.; Lalji, S.M. Performance of asphaltene stability predicting models in field environment and development of new stability predicting model (ANJIS). *J. Pet. Explor. Prod. Technol.* **2022**, *12*, 1423–1436. [[CrossRef](#)]
39. Jamaluddin, A.K.M.; Creek, J.; Kabir, C.S.; McFadden, J.D.; D’Cruz, D.; Manakalathil, J.; Joshi, N.; Ross, B. Laboratory techniques to measure thermodynamic asphaltene instability. *J. Can. Pet. Technol.* **2002**, *41*, 44–52. [[CrossRef](#)]
40. Akbarzadeh, K.; Hammami, A.; Kharrat, A.; Zhang, D. Asphaltenes—Problematic but rich in potential. *Oilfield Rev.* **2007**, *19*, 22–43.
41. Pereira, V.J.; Setaro, L.L.O.; Costa, G.M.N.; Vieira De Melo, S.A.B. Evaluation and improvement of screening methods applied to asphaltene precipitation. *Energy Fuels* **2017**, *31*, 3380–3391. [[CrossRef](#)]
42. Rogel, E.; Ovalles, C.; Vien, J.; Moir, M. Asphaltene solubility properties by the in-line filtration method. *Energy Fuels* **2015**, *29*, 6363–6369. [[CrossRef](#)]
43. Castillo, M.A.; Rueda-Chacón, H.; Agudelo, J.L.; Molina, V.D. Prediction of the stability and compatibility of colombian heavy crude oils by 1D low field nuclear magnetic resonance relaxometry and chemometric methods. *Fuel* **2021**, *298*, 120721. [[CrossRef](#)]
44. Castillo, M.A.; Páez, A.A.; Rueda-Chacón, H.; Agudelo, J.L.; Molina, V.D. Prediction of the insolubility number and the solubility blending number of colombian heavy crude oils by 1H nuclear magnetic resonance and partial least squares. *Energy Fuels* **2019**, *34*, 1592–1600. [[CrossRef](#)]
45. Escobedo, J.; Mansoori, G.A. Viscometric determination of the onset of asphaltene flocculation: A novel method. *SPE Prod. Fac.* **1995**, *10*, 115–118. [[CrossRef](#)]
46. Adeyanju, O.A.; Adeosun, T.A.; Obisanya, A.A. Experimental study of viscosity as a criterion for determination of onset of asphaltene flocculation in Nigeria’s crude. *Pet. Coal.* **2015**, *57*, 601–608.
47. Fakher, S.; Yousef, A.; Al-Sakkaf, A.; Eldaka, S. Asphaltene onset pressure measurement and calculation techniques: A review. *Petroleum* **2023**. [[CrossRef](#)]
48. Soleymanzadeh, A.; Yousefi, M.; Kord, S.; Mohammadzadeh, O. A review on methods of determining onset of asphaltene precipitation. *J. Pet. Explor.* **2018**, *9*, 1375–1396. [[CrossRef](#)]

49. Ali, S.I.; Lalji, S.M.; Haneef, J.; Ahsan, U.; Tariq, S.M.; Tirmizi, S.T.; Shamim, R. Critical analysis of different techniques used to screen asphaltene stability in crude oils. *Fuel* **2021**, *299*, 120874. [[CrossRef](#)]
50. Van den Berg, F.; Kapusta, S.; Ooms, A.; Smith, A. Fouling and compatibility of crudes as basis for a new crude selection strategy. *Pet. Sci. Technol.* **2003**, *21*, 557–568. [[CrossRef](#)]
51. Wiehe, I.A.; Kennedy, R.J. Process for Blending Potentially Incompatible Petroleum Oils. ExxonMobil Technology and Engineering Co. U.S. Patent US5871634A, 16 February 1999.
52. Rahimi, P.; Alem, T. Crude oil compatibility and diluent evaluation for pipelining. In Proceedings of the Crude Oil Quality Association Meeting, New Orleans, LA, USA, 9 February 2010.
53. Evdokimov, I. The importance of asphaltene content in petroleum III—new criteria for prediction of incompatibility in crude oil blends. *Pet. Sci. Technol.* **2010**, *28*, 1351–1357. [[CrossRef](#)]
54. Rogel, E.; Hench, K.; Cibotti, F.; Forbes, E.; Jackowski, L. Investigation on crude oil fouling behavior. *Energy Fuels* **2022**, *36*, 818–825. [[CrossRef](#)]
55. Jiguang, L.; Huandi, H.; Haiping, S. A new insight into compatibility changing rules for inferior vacuum residue’s thermal cracking and hydrocracking process. *J. Anal. Appl. Pyrolysis* **2022**, *167*, 105632. [[CrossRef](#)]
56. Dickakian, G.B. Blending of Hydrocarbon Liquids. U.S. Patent 4853337, 1 August 1989.
57. Ho, T.C. A study of crude oil fouling propensity. *Int. J. Heat. Mass. Transf.* **2016**, *95*, 62–68. [[CrossRef](#)]
58. Sultanbekov, R.R.; Schipachev, A.M. Manifestation of incompatibility of marine residual fuels: A method for determining compatibility, studying composition of fuels and sediment. *J. Min. Inst.* **2022**, *257*, 843–852. [[CrossRef](#)]
59. Sultanbekov, R.; Islamov, S.; Mardashov, D.; Beloglazov, I.; Hemmingsen, T.; Pérez, D.E.; López-Gutiérrez, J.-S.; Negro, V.; Graça Neves, M. Research of the influence of marine residual fuel composition on sedimentation due to incompatibility. *J. Mar. Sci. Eng.* **2021**, *9*, 1067–1081. [[CrossRef](#)]
60. Fakher, S.; Ahdaya, M.; Elturki, M.; Imqam, A. Critical review of asphaltene properties and factors impacting its stability in crude oil. *J. Pet. Explor.* **2019**, *10*, 1183–1200. [[CrossRef](#)]
61. Hernández, E.A.; Lira-Galeana, C.; Ancheyta, J. Analysis of asphaltene precipitation models from solubility and thermodynamic-colloidal theories. *Processes* **2023**, *11*, 765–788. [[CrossRef](#)]
62. Bambinek, K.; Przyjazny, A.; Boczkaj, G. Compatibility of crude oil blends—processing issues related to asphaltene precipitation, methods of instability prediction—A review. *Ind. Eng. Chem. Res.* **2023**, *62*, 2–15. [[CrossRef](#)]
63. Patil, P.D.; Kozminski, M.; Peterson, J.; Kumar, S. Fouling diagnosis of pennsylvania grade crude blended with opportunity crude oils in a refinery crude unit’s hot heat exchanger train. *Ind. Eng. Chem. Res.* **2019**, *58*, 17918–17927. [[CrossRef](#)]
64. Rogel, E.; Hench, K.; Hajdu, P.; Ingham, H. The role of compatibility in determining the blending and processing of crude oils. In *Chemistry Solutions to Challenges in the Petroleum Industry*; ACS Symposium Series; American Chemical Society: Washington, DC, USA, 2019; Volume 1320, pp. 201–222.
65. Shishkova, I.K.; Stratiev, D.S.; Tavlieva, M.P.; Dinkov, R.K.; Yordanov, D.; Sotirov, S.; Sotirova, E.; Atanassova, V.; Ribagin, S.; Atanassov, K.; et al. Evaluation of the different compatibility indices to model and predict oil colloidal stability and its relation to crude oil desalting. *Resources* **2021**, *10*, 75–95. [[CrossRef](#)]
66. Nemana, S.; Kimbrell, R.M.; Zaluzec, E. Predictive Crude Oil Compatibility Model. U.S. Patent 7618822B2, 30 October 2007.
67. Ali, S.I.; Lalji, S.M.; Awan, Z.; Qasim, M.; Alshahrani, T.; Khan, F.; Ullah, S.; Ashraf, A. Prediction of asphaltene stability in crude oils using machine learning algorithms. *Chemom. Intell. Lab. Syst.* **2023**, *235*, 104784. [[CrossRef](#)]
68. Malkin, A.; Rodionova, G.; Simon, S.; Ilyin, S.O.; Arinina, M.P.; Kulichikhin, V.G.; Sjöblom, J. Some Compositional Viscosity Correlations for Crude Oils from Russia and Norway. *Energy Fuels* **2016**, *30*, 9322–9328. [[CrossRef](#)]
69. Jia, B.; Xian, C.; Jia, W.; Su, J. Improved Petrophysical Property Evaluation of Shaly Sand Reservoirs Using Modified Grey Wolf Intelligence Algorithm. *Comput. Geosci.* **2023**, *27*, 537–549. [[CrossRef](#)]
70. Jia, B.; Xian, C.; Tsau, J.-S.; Zuo, X.; Jia, W. Status and Outlook of Oil Field Chemistry-Assisted Analysis during the Energy Transition Period. *Energy Fuels* **2022**, *36*, 12917–12945. [[CrossRef](#)]
71. ASTM D4052-22; Standard Test Method for Density, Relative Density, and Api Gravity of Liquids by Digital Density Meter. ASTM International: West Conshohocken, PA, USA, 2022; Volume 05.01.
72. ASTM D4294; Standard Test Method for Sulfur in Petroleum and Petroleum Products by Energy Dispersive X-ray Fluorescence Spectrometry. ASTM International: West Conshohocken, PA, USA, 2021; Volume 05.02.
73. Stratiev, D.; Shishkova, I.; Dinkov, R.; Dobrev, D.; Argirov, G.; Yordanov, D. *The Synergy between Ebullated Bed Vacuum Residue Hydrocracking and Fluid Catalytic Cracking Processes in Modern Refining—Commercial Experience*; Professor Marin Drinov Publishing House of Bulgarian Academy of Sciences: Sofia, Bulgaria, 2022.
74. IP 501/05; Determination of Aluminium, Silicon, Vanadium, Nickel, Iron, Sodium, Calcium, Zinc and Phosphorus in Residual Fuel Oil by Ashing, Fusion and Inductively Coupled Plasma Emission Spectrometry. Energy Institute: London, UK, 2019.
75. ASTM D2892; Standard Test Method for Distillation of Crude Petroleum (15-Theoretical Plate Column). ASTM International: West Conshohocken, PA, USA, 2020; Volume 05.01.
76. ASTM D5236-18A; Standard Test Method for Distillation of Heavy Hydrocarbon Mixtures (Vacuum Potstill Method). ASTM International: West Conshohocken, PA, USA, 2018; Volume 05.02.

77. ASTM D7169-20e1; Standard Test Method for Boiling Point Distribution of Samples with Residues such as Crude Oils and Atmospheric and Vacuum Residues by High Temperature Gas Chromatography. ASTM International: West Conshohocken, PA, USA, 2020; Volume 05.03.
78. He, P.; Ghoniem, A.F. A group contribution pseudocomponent method for phase equilibrium modeling of mixtures of petroleum fluids and a solvent. *Ind. Eng. Chem. Res.* **2015**, *54*, 8809–8820. [[CrossRef](#)]
79. Vakili-Nezhaad, G.R.; Modarress, H. A New Characterization Factor for Hydrocarbons and Petroleum Fluids Fractions. *Oil Gas. Sci. Technol. Rev. IFP* **2002**, *57*, 149–154.
80. Whitson, C. Characterizing hydrocarbon plus fractions. *Soc. Pet. Eng. J.* **1983**, *23*, 683–694. [[CrossRef](#)]
81. Watson, K.; Nelson, E. Improved methods for approximating critical and thermal properties of petroleum fractions. *Ind. Eng. Chem.* **1933**, *25*, 880–887. [[CrossRef](#)]
82. Gharagheizi, F.; Fazeli, A. Prediction of the watson characterization factor of hydrocarbon components from molecular properties. *QSAR Comb. Sci.* **2008**, *27*, 758–767. [[CrossRef](#)]
83. Mohammadi, A.; Omidkhah, M.; Karimzadeh, R.; Haghtalab, A. Structural modeling of petroleum fractions based on mixture viscosity and Watson K factor. *Korean J. Chem. Eng.* **2013**, *30*, 465–473. [[CrossRef](#)]
84. Herrera, S.; Merlino, M.; Di Lullo, A.; Merino-Garcia, D. Estimation of the solvent power of crude oil from density and viscosity measurements. *Ind. Eng. Chem. Res.* **2005**, *44*, 9307–9315. [[CrossRef](#)]
85. Atanassov, K.; Mavrov, D.; Atanassova, V. InterCriteria decision making: A new approach for multicriteria decision making, based on index matrices and intuitionistic fuzzy sets. *Issues Intuitionistic Fuzzy Sets Gen. Nets* **2014**, *11*, 1–8.
86. Atanassov, K.; Marinov, P.; Atanassova, V. InterCriteria analysis with interval-valued intuitionistic fuzzy evaluations. In *Flexible Query Answering Systems; Lecture Notes in Computer Science; Cuzzocrea, A., Greco, S., Larsen, H., Saccà, D., Andreasen, T., Christiansen, H., Eds.; Springer: Berlin/Heidelberg, Germany, 2019; Volume 11529, pp. 329–338.*
87. Atanassov, K.; Atanassova, V.; Gluhchev, G. InterCriteria analysis: Ideas and problems. *Notes Intuitionistic Fuzzy Sets* **2015**, *21*, 81–88.
88. Stratiev, D.; Shishkova, I.; Dinkov, R.; Kolev, I.; Argirov, G.; Ivanov, V.; Ribagin, S.; Atanassova, V.; Atanassov, K.; Stratiev, D.D.; et al. InterCriteria analysis to diagnose the reasons for increased fouling in a commercial ebullated bed vacuum residue hydrocracker. *ACS Omega* **2022**, *7*, 30462–30476. [[CrossRef](#)] [[PubMed](#)]
89. Qi, Y.; Cai, C.F.; Sun, P.; Wang, D.W.; Zhu, H.J. Crude oil cracking in deep reservoirs: A review of the controlling factors and estimation methods. *Pet. Sci.* **2023**, *20*, 1978–1997. [[CrossRef](#)]
90. Viswanathan, B.P. *Energy Sources: Fundamentals of Chemical Conversion Processes and Applications*; Elsevier: Amsterdam, The Netherlands, 2017; pp. 29–57.
91. Vandembroucke, M.; Largeau, C. Kerogen origin, evolution and structure. *Org. Geochem.* **2007**, *38*, 719–833. [[CrossRef](#)]
92. Behar, F.; Vandembroucke, M.; Tang, Y.; Marquis, F.; Espitalie, J. Thermal cracking of kerogen in open and closed systems: Determination of kinetic parameters and stoichiometric coefficients for oil and gas generation. *Org. Geochem.* **1997**, *26*, 321–339. [[CrossRef](#)]
93. Donadelli, J.A.; Pineda, J.; Comerio, M.; Smal, C.; Erra, G.; Acost, R.H.; Delfa, G.M. Natural and laboratory-induced maturation of kerogen from the Vaca Muerta Formation: A comparison study. *Org. Geochem.* **2023**, *185*, 104690. [[CrossRef](#)]
94. Gama, J.; Schwark, L. Assessment of kerogen types and source rock potential of lower jurassic successions in the Mandawa basin, SE Tanzania. *Mar. Pet. Geol.* **2023**, *157*, 106505. [[CrossRef](#)]
95. Salter, T.L.; Watson, J.S.; Sephton, M.A. Effects of minerals (phyllosilicates and iron oxides) on the responses of aliphatic hydrocarbon containing kerogens (type I and type II) to analytical pyrolysis. *J. Anal. Appl. Pyrolysis* **2023**, *170*, 105900. [[CrossRef](#)]
96. Liu, B.; Mohammadi, M.-R.; Ma, Z.; Bai, L.; Wang, L.; Wen, Z.; Liu, Y.; Morta, H.B.; Hemmati-Sarapardeh, A.; Ostadhassan, M. Experimental investigation and intelligent modeling of pore structure changes in type III kerogen-rich shale artificially matured by hydrous and anhydrous pyrolysis. *Energy* **2023**, *282*, 128799. [[CrossRef](#)]
97. Safaei-Farouji, M.; Liu, B.; Gentzis, T.; Wen, Z.; Ma, Z.; Bai, L.; Ostadhassan, M. Geochemical evolution of kerogen type III during hydrous pyrolysis: A case study from the damoguaihe formation, Hailar basin, China. *Geoenergy Sci. Eng.* **2023**, *228*, 211947. [[CrossRef](#)]
98. Li, X.; Xie, H.; Birdwell, J.E.; McGovern, G.P.; Horita, J. Intramolecular carbon isotope geochemistry of butane isomers from laboratory maturation and Monte-Carlo simulations of kerogen types I, II, and III. *Geochim. Cosmochim. Acta* **2023**, *360*, 57–67. [[CrossRef](#)]
99. Lu, C.; Xiao, X.; Gai, H.; Feng, Y.; Li, G.; Meng, G.; Gao, P. Nanopore structure characteristics and evolution of type III kerogen in marine-continental transitional shales from the Qinshui basin, Northern China. *Geoenergy Sci. Eng.* **2023**, *221*, 211413. [[CrossRef](#)]
100. Hui, S.S.; Pang, X.Q.; Jiang, F.J.; Wang, C.X.; Mei, S.X.; Hu, T.; Pang, H.; Li, M.; Zhou, X.L.; Shi, K.Y. Quantitative effect of kerogen type on the hydrocarbon generation potential of paleogene lacustrine source rocks, Liaohe Western Depression, China. *Pet. Sci.* **2024**, *21*, 14–30. [[CrossRef](#)]
101. Liang, T.; Zhan, Z.W.; Zou, Y.R.; Lin, X.H.; Shan, Y.; Peng, P. Research on type I kerogen Molecular simulation and docking between kerogen and saturated hydrocarbon molecule during oil generation. *Chem. Geol.* **2023**, *617*, 121263. [[CrossRef](#)]
102. Zheng, X.; Sanei, H.; Schovsbo, N.H.; Luo, Q.; Wu, J.; Zhong, N.; Galloway, J.M.; Goodarzi, F. Role of zooclasts in the kerogen type and hydrocarbon potential of the lower paleozoic alum shale. *Int. J. Coal. Geol.* **2021**, *248*, 103865. [[CrossRef](#)]

103. Stratiev, D.; Dinkov, R.; Shishkova, I.; Yordanov, D. Can we manage the process of asphaltene precipitation during the production of IMO 2020 Fuel Oil? *Erdoel Erdgas Kohle* **2020**, *12*, 32–39.
104. Lehne, E.; Dieckmann, V. Bulk kinetic parameters and structural moieties of asphaltenes and kerogens from a sulphur-rich source rock sequence and related petroleums. *Org. Geochem.* **2007**, *38*, 1657–1679. [[CrossRef](#)]
105. Dhulesia, H. New correlations predict FCC feed characterizing parameters. *Oil Gas. J.* **1986**, *84*, 51–54.
106. Bahonar, E.; Chahardowli, M.; Ghalenoei, Y.; Simjoo, M. New correlations to predict oil viscosity using data mining techniques. *J. Pet. Sci. Eng.* **2022**, *208*, 109736. [[CrossRef](#)]
107. Hadavimoghaddam, F.; Ostadhassan, M.; Heidaryan, E.; Sadri, M.A.; Chapanova, I.; Popov, E.; Cheremisin, A.; Rafieepour, S. Prediction of dead oil viscosity: Machine learning vs. classical correlations. *Energies* **2021**, *14*, 930–946. [[CrossRef](#)]
108. Stratiev, D.; Shishkova, I.; Dinkov, R.; Nenov, S.; Sotirov, S.; Sotirova, E.; Kolev, I.; Ivanov, V.; Ribagin, S.; Atanassov, K.; et al. Prediction of petroleum viscosity from molecular weight and density. *Fuel* **2023**, *331*, 125679. [[CrossRef](#)]
109. Stratiev, D.; Sotirov, S.; Sotirova, E.; Nenov, S.; Dinkov, R.; Shishkova, I.; Kolev, I.V.; Yordanov, D.; Vasilev, S.; Atanassov, K.; et al. Prediction of molecular weight of petroleum fluids by empirical correlations and artificial neuron networks. *Processes* **2023**, *11*, 426. [[CrossRef](#)]
110. Palichev, G.N.; Stratiev, D.; Sotirov, S.; Sotirova, E.; Nenov, S.; Shishkova, I.; Dinkov, R.; Atanassov, K.; Ribagin, S.; Stratiev, D.D.; et al. Prediction of refractive index of petroleum fluids by empirical correlations and ANN. *Processes* **2023**, *11*, 2328. [[CrossRef](#)]
111. Stratiev, D.; Nenov, S.; Shishkova, I.; Sotirov, S.; Sotirova, E.; Dinkov, R.; Yordanov, D.; Pilev, D.; Atanassov, K.; Vasilev, S. Prediction of viscosity of blends of heavy oils with diluents by empirical correlations and artificial neural network. *Ind. Eng. Chem. Res.* **2023**, *62*, 21449–21463. [[CrossRef](#)]
112. Braimah, M.N. Application of artificial neural network (ANN) in the optimization of crude oil refinery process: New Port-Harcourt Refinery. *J. Energy Res. Rev.* **2020**, *5*, 26–38. [[CrossRef](#)]
113. Ore, O.T.; Adebiyi, F.M. Pyrolysis of Oil Sand Bitumen Using a Fixed-Bed Reactor: Process Modeling and Compositional Analysis. *Ind. Eng. Chem. Res.* **2024**, *62*, 14151–14166. [[CrossRef](#)]
114. Lighter Crude Slate Restricts European Refiners. Available online: <https://www.argusmedia.com/en/news-and-insights/latest-market-news/2478828-lighter-crude-slate-restricts-european-refiners> (accessed on 15 March 2024).
115. Ranaee, E.; Ghorbani, H.; Keshavarzian, S.; Abarghoei, P.G.; Riva, M.; Fabio Inzoli, F.; Guadagnini, A. Analysis of the performance of a crude-oil desalting system based on historical data. *Fuel* **2021**, *291*, 120046. [[CrossRef](#)]
116. Pereira, J.; Velasquez, I.; Blanco, R.; Sanchez, M.; Pernalet, C.; Canelón, C. Chapter 4. Crude Oil Desalting Process. Available online: <https://cdn.intechopen.com/pdfs/48963.pdf> (accessed on 18 March 2024).
117. Treese, S.A.; Pujado, P.R.; Jones, D.S.J. *Handbook of Petroleum Processing*, 2nd ed.; Springer: Cham, Switzerland, 2015.
118. Abdel-AalMohammed, H.K.; Alsahlawi, A. *Petroleum Economics and Engineering*, 3rd ed.; Taylor & Francis Group: Abingdon, UK, 2014.
119. Kaiser, M.J.; De Klerk, A.; Gary, J.H.; Handwerk, G.E. *Petroleum Refining. Technology, Economics, and Markets*, 6th ed.; CRC Press: Boca Raton, FL, USA, 2020.

Disclaimer/Publisher's Note: The statements, opinions and data contained in all publications are solely those of the individual author(s) and contributor(s) and not of MDPI and/or the editor(s). MDPI and/or the editor(s) disclaim responsibility for any injury to people or property resulting from any ideas, methods, instructions or products referred to in the content.